Soft Computing
https://doi.org/10.1007/s00500-023-09456-3

FOCUS

The effect of the pandemic on complex socio-economic systems: community detection induced by communicability

Gian Paolo Clemente[1] · Rosanna Grassi[2] · Giorgio Rizzini[3]

Accepted: 7 November 2023

Abstract
In this paper, we aim at investigating various aspects of countries' behaviour during the coronavirus pandemic period. By means of a multiplex network, we simultaneously consider government responses based on COVID-19 infections, Stringency Index, international trade and international air mobility data, to detect clusters of countries that showed a similar reaction to the pandemic. We propose a new methodological approach based on the Estrada communicability for identifying communities on a multiplex network, based on a two-step optimization process. At first, we determine the optimal inter-layer weight between levels by minimizing a distance function. Hence, the optimal weight is used to detect the communities on each layer. Our findings show that this new approach to community detection on a multiplex network provides additional insights with respect to the same procedure performed on layers separately. Indeed, clusters in the multiplex network benefit from a higher cohesion, as they are detected taking into account the mutual influence of the other networks.

Keywords Multiplex networks · Community detection · Communicability distance · Socio-economic networks

1 Introduction

There is a clear relationship between COVID-19 disease, containment measures, and socio-economic factors, as pointed out in Paez et al. (2020), Sharma et al. (2021), Sha et al. (2020). The COVID-19 pandemic occurred in a globally interconnected system involving several aspects of human life. At the beginning of the pandemic, the socio-economic framework contributed to spread the disease. Indeed, the flow of people travelling around the world or spending time together favoured virus diffusion [see, e.g. Antonietti et al. (2021), Al-Salem et al. (2021), Fernández-Villaverde and Jones (2020)]. Some factors link wealth with the COVID-19 pandemic, such as the age of people in different countries, the international flows of goods and tourists, and the endowment of the health facilities. These aspects reasonably played an important role in spreading the infection.

For these reasons, the containment measures adopted by countries had an impact on these contexts. To rapidly face the pandemic, policymakers dealt with the trade-off between safeguarding public health and mitigating the negative economic impact of epidemic containment measures [see, e.g. Cross et al. (2020), Federico and Ferrari (2021), Barbero et al. (2021), Kok (2020), Baig et al. (2021)].

These reasons naturally lead to investigate this complex system with network tools exploiting the mathematical properties and the characteristics of multiplex networks. In this way, we take into account simultaneously different facets of COVID-19 diffusion [see Montes-Orozco et al. (2020) for interesting insights on this issue]. To this end, we aim at detecting communities of countries that showed a similar reaction to the pandemic. Community detection is not an easy task in a complex system. At a global level, the system can appear as a dense and compact set of relations, so that the mesoscale structure does not easily emerge.

✉ Rosanna Grassi
rosanna.grassi@unimib.it

Gian Paolo Clemente
gianpaolo.clemente@unicatt.it

Giorgio Rizzini
giorgio.rizzini@sns.it

[1] Dipartimento di Matematica per le Scienze Economiche, Finanziarie ed Attuariali, Università Cattolica del Sacro Cuore, Via Necchi, 9, 20123 Milan, Italy

[2] Dipartimento di Statistica e Metodi Quantitativi, Università degli Studi di Milano-Bicocca, via Bicocca degli Arcimboldi, 8, 20216 Milan, Italy

[3] Classe di Scienze, Scuola Normale Superiore, Piazza dei Cavalieri, 56100 Pisa, Italy

Published online: 20 December 2023

In this context, the concept of distance between nodes plays an important role, since nodes distant from a given one can influence it while passing through intermediary ones. Recently, Bartesaghi et al. (2022) proposed an innovative methodology to detect communities based on the Estrada communicability distance [see Estrada and Hatano (2009); Estrada (2019)]. Differently from the classical Euclidean distance, the proposed measure also considers indirect connections becoming crucial to catch deep interconnections between nodes.

Starting from this idea, we propose a methodology to detect communities in a multiplex framework. Connections between nodes in a layer determine not only the topology of the network in that layer, but also mutually influence the structures of the other layers. Communities in each layer of the multiplex are then affected also by the strength of connections with the other layers. We propose a procedure that considers this aspect by introducing a weight on the links between the different layers. We set this weight in a way that minimizes the average distance of the entire multiplex, expressing the high propensity to communicate between nodes of the various layers. Then, on the multiplex network we perform a community detection on each layer, based on the Estrada communicability distance.

Detected communities in this way incorporate the mutual influence of the other layers. Indeed, traditional methods of network analysis, while effective in capturing individual layers of interaction, fall short in capturing the intricate interplay between these layers. By considering layers independently, we overlook the rich tapestry of interdependencies that exist across the networks. Therefore, this proposal, based on multiplex network, overcomes the limitations of traditional single–layer network and allows us to unveil the hidden layers of interconnectedness and provide a more comprehensive understanding of the complex system. It enables indeed to comprehend how different layers interact, influence one another, and collectively shape the behaviour and evolution of the whole system. In particular, the proposed approach is applied to a multiplex network describing various aspects of the pandemic, namely the effect of the containment measures, represented by the Stringency Index values, the COVID-19 infections, the international trade data, and the air mobility data. Indeed, classical approaches based on single-layer do not consider that entities can interact simultaneously in many ways. In a multiplex, communities have to be affected not only by the topological structure of the network in each layer, but also by inter-layer connections.

Since on each layer we describe the interrelationship between countries by looking at a specific aspect, to compare heterogeneous data we unify the representation through the correlations between countries. Specifically, we build the correlation matrix between countries that quantify their similarity, and then we extract the multiplex network by filtering the non-significant correlations under a p-value threshold of 5%.

In general, filtering the correlations is a widely used method for generating networks from correlation matrices. The threshold-based approach is one of the most popular, and several criteria for selecting the threshold value have been proposed [see Onnela et al. (2004), Boginski et al. (2005), Zanin et al. (2012), De Vico Fallani et al. (2017)]. Other filtering procedures are based on a geometric approach, exploiting suitable properties of some metric spaces. This is the case, for instance, of the search of the minimal spanning tree obtained from the strongest correlations (Mantegna and Stanley 1999; Mantegna 1999), or the planar maximally filtered graph [see Hyde (2005), Tumminello et al. (2005)]. Many variants to improve these methods can be found in the literature; for an exhaustive survey, the reader can refer to Marti et al. (2021).

Since the pandemic broke out, some works studied the connections between the commercial trades and the COVID-19 diffusion using network tools [see, e.g. Antonietti et al. (2020), Reissl et al. (2022), Kiyota (2022), Fagiolo (2020)]. Differently from Antonietti et al. (2021) that investigates the effect on the socio-economic framework of the first wave of COVID-19 pandemic, our approach allows to analyse the COVID-19 infection taking jointly into account the adoption of diversified containment policies, the international trades, as well as the mobility.

As a result, we obtain a lower number of communities on each layer, ensuring a higher cohesion with respect to the one that would be obtained focusing only on single layers. On COVID-19 and Stringency Index layers, a world split into two part emerges. In particular, we group together countries in which COVID-19 has been detected in the first period and characterized by a prompt reaction of the policymakers.

The international trade network layer is featured by a strong persistence in the mesoscale structure. Indeed, we argue that the pandemic effect of the first wave did not have an impact on medium-long run connections between countries, strengthening the geographical relationships. In the international air mobility layer two distinct behaviours emerge: a cluster with countries marginally touched by the contagion and a second group of countries strongly involved in the pandemic scenario.

The paper is organized as follows. In Sect. 2, we remind some preliminary definitions and the Estrada communicability distance. In Sect. 3, we explain the two-step optimization procedure. In Sect. 4, we construct the multiplex network based on the data, and in Sect. 4.3 we discuss the results. Section 5 reports the conclusions. Appendix A provides an alternative expression of the distance function and Appendix B presents the proof of the theorem. In Appendix C, we report an analysis of the proposed methodology by means of three simple examples. In Appendix D and E, the reader can find the list of countries and layers representation.

2 Communicability in multiplex networks

2.1 Preliminary definitions

A network is formally represented by a graph $G = (V, E)$, where V is the set of n nodes and E is the set of m edges (or links). Two nodes are adjacent if an edge $(i, j) \in E$ exists between them. The network is assumed to be undirected, i.e. (j, i) is an element of E whenever (i, j) is such. The adjacency relations among all nodes are collected into a symmetric $n \times n$ matrix $\mathbf{A}$ (adjacency matrix). No self-loops are allowed, that is, $a_{ii} = 0$ for $i = 1, \ldots, n$. A $i - j$-walk is a sequence of vertices and edges between i and j. If vertices are distinct, the walk is said to be a path. The length of a walk is the number of its edges (including the repeated ones). A graph G is connected if, $\forall i, j \in V$, a $i - j$-path connecting them exists. From now on, we assume to deal with a connected graph.

If a non-negative real number w_{ij} is associated with each edge (i, j), we say that the graph is weighted. The weighted relations among all nodes are collected into a $n \times n$ matrix $\mathbf{W}$, called weighted adjacency matrix. For further details, the reader can refer to Estrada (2012b).

The above definitions can be extended to multiplex networks [see Estrada and Gómez-Gardeñes (2014) and Cozzo et al. (2018)]. Formally, a multiplex network M (multiplex, for short) is defined by a set of h networks $G_\alpha = (V, E_\alpha)$, $\alpha = 1, \ldots, h$ and a family of sets $E_{\alpha,\beta}$, with $\alpha, \beta = 1, \ldots, h$ and $\alpha \neq \beta$ of links such that each link connects a node of G_α with its replica in the graph G_β. Each network G_α is then located into a layer α and two networks G_α and G_β are connected by links of the set $E_{\alpha,\beta}$. Notice that two nodes can be coupled through different types of connections, namely intra-layer and inter-layer connections. The intra-layer connection refers to the link that connects any two nodes on the same layer, while the inter-layer link connects a node with itself in different layers. A graphical representation of a multiplex is provided in Fig. 1.

The topology of a multiplex network is completely described by the supradjacency matrix $\mathcal{A}$ defined by

$$\mathcal{A} = \begin{pmatrix} \mathbf{A}_1 & \mathbf{0} & \ldots & \mathbf{0} \\ \mathbf{0} & \mathbf{A}_2 & \ldots & \mathbf{0} \\ \vdots & \vdots & \ddots & \vdots \\ \mathbf{0} & \mathbf{0} & \ldots & \mathbf{A}_h \end{pmatrix} + \begin{pmatrix} 0 & \mathbf{C}_{12} & \ldots & \mathbf{C}_{1h} \\ \mathbf{C}_{21} & 0 & \ldots & \mathbf{C}_{2h} \\ \vdots & \vdots & \ddots & 0 \\ \mathbf{C}_{h1} & \mathbf{C}_{h2} & \ldots & 0 \end{pmatrix} = \mathbf{A}_L + \mathbf{C}_{LL},$$

with $\mathbf{A}_L$ being the block matrix of the adjacency matrices of each layer $\mathbf{A}_\alpha, \alpha = 1, \ldots, h$ and $\mathbf{C}_{LL}$ the block matrix of all the inter-layer connections between layers. Each element of $\mathbf{C}_{LL}$ is a matrix representing the connections between corresponding nodes in different layers. Analogously, we can define a weighted supradjacency matrix $\mathcal{W} = \mathbf{W}_L + \mathbf{C}_{LL}$, where $\mathbf{W}_L$ is the block matrix of the weighted adjacency matrices $\mathbf{W}_\alpha, \alpha = 1, \ldots, h$.

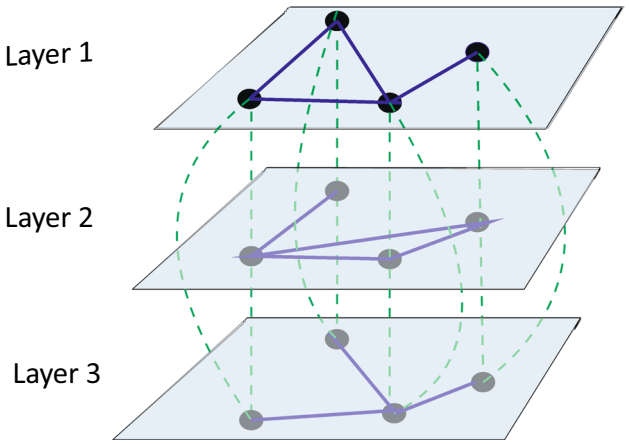

Fig. 1 A multiplex network with three layers and four nodes. Blue links are the intra-layer connections. Green dashed links are the inter-layer connections

As standing hypotheses, we assume that the weighted adjacency matrices $\mathbf{W}_\alpha$ have weights $w_{ij,\alpha} \in [0, 1]$ and, as in Estrada (2019), $\mathbf{C}_{\alpha\beta} = \mathbf{C}_{\beta\alpha} = \omega\mathbf{I}\ \forall\alpha, \beta$, where ω is a positive real parameter that expresses the weight of inter-layer connections and $\mathbf{I}$ is the n-square identity matrix. Note that ω expresses the intensity of a connection between two nodes lying on two different layers: low (high) values of ω indicate a weak (strong) connection between them.[1]

In particular, $\omega = 0$ corresponds to the case in which all layers are independent, i.e. each layer does not influence the other ones. In this case, the multiplex becomes a set of single-layer networks, not interrelated to each other. On the contrary, a positive value for ω makes that, simultaneously, each layer influences and is influenced by the other ones. We assume that $\omega \in [0, 1]$ to ensure that the inter-layer connections have the same order of magnitude of the intra-layer links allowing the comparability between them.

2.2 Estrada communicability distance

We are interested in analysing how a pair of nodes communicate in a multiplex. To this end, we use the definition of network communicability introduced by Estrada (2012a) and then extended to multiplex networks in Estrada and Gómez-Gardeñes (2014).

Formally, given a multiplex described by a supradjacency matrix $\mathcal{A}$, the Estrada communicability (communicability,

[1] We stress that each layer α can influence the others through inter-layer weights that can be, in general, different. For the sake of simplicity and for analytical tractability of the problem, in this paper we assign to all layers a unique inter-layer value identified by ω.

for short) between nodes i and j is defined as:

$$G_{ij} = \sum_{k=0}^{\infty} \frac{1}{k!} [\mathcal{A}^k]_{ij} = \left[\exp(\mathcal{A}) \right]_{ij}. \quad (1)$$

By means of the $k-$th power of $\mathcal{A}$, formula (1) provides the number of walks of length k starting from i and arriving at j, giving more importance (by the factor $k!$) to the shortest walks connecting them. G_{ij} represents the flow of information passing between two nodes i and j, possibly located in different layers.[2] When $i = j$, the quantity G_{ii} is known in the literature as subgraph centrality [see Estrada and Rodriguez-Velazquez (2005)]. This measure represents the importance of a node i with respect to the number of closed walks starting from the node and returning to the same node.

To extend the definition of communicability to the weighted case, following Estrada (2012b) and Crofts and Higham (2009), we first normalize the matrix $\mathcal{W}$ as $\mathcal{S}^{-\frac{1}{2}} \mathcal{W} \mathcal{S}^{-\frac{1}{2}}$, where $\mathcal{S}$ is a nh-square diagonal matrix containing the strengths of the nodes for each layer. Then the Estrada communicability (for weighted multiplex networks) is defined as:

$$G_{ij} = \sum_{k=0}^{\infty} \frac{1}{k!} \left[\left(\mathcal{S}^{-\frac{1}{2}} \mathcal{W} \mathcal{S}^{-\frac{1}{2}} \right)^k \right]_{ij} = \left[\exp\left(\mathcal{S}^{-\frac{1}{2}} \mathcal{W} \mathcal{S}^{-\frac{1}{2}} \right) \right]_{ij}. \quad (2)$$

In this case, the Estrada communicability between nodes i and j represents the number of weighted walks connecting them. The weight of each walk is the product of the weights of all edges involved in it including their repetition.

It is worth noting that in the multiplex case, the Estrada communicability G_{ij} between nodes i and j does not consider only the intra-layer connections, as in the case of single-layer networks, but also the inter-layer connections. Therefore, it crucially depends on how layers are connected, and hence, at the end, on the weight ω.

The communicability matrix $\mathcal{G}$ is a block matrix defined as

$$\mathcal{G} = \exp(\mathcal{S}^{-\frac{1}{2}} \mathcal{W} \mathcal{S}^{-\frac{1}{2}}) = \begin{pmatrix} \mathbf{G}_1 & \mathbf{G}_{12} & \dots & \mathbf{G}_{1h} \\ \mathbf{G}_{21} & \mathbf{G}_2 & \dots & \mathbf{G}_{2h} \\ \vdots & \vdots & \ddots & \vdots \\ \mathbf{G}_{h1} & \mathbf{G}_{h2} & \dots & \mathbf{G}_h \end{pmatrix}. \quad (3)$$

Matrix $\mathbf{G}_{\alpha\beta}$, $\alpha, \beta = 1, \dots, h$ is an n-square matrix representing the communicability between a node in the layer α and itself in layer β, while $\mathbf{G}_\alpha$ reports the communicability between every pair of nodes in layer α.

[2] As explained in Estrada and Hatano (2008), information is intended in broad sense to indicate any kind of flow along edges, such as money, current, traffic, and so on.

Using the communicability in formulas (1) or (2), it is possible to define a suitable metric between couple of nodes, namely the communicability distance $\xi_{ij} = G_{ii} + G_{jj} - 2G_{ij}$ [see Estrada and Hatano (2008) and Estrada (2019)], which measures how two nodes are distant in communicating, wherever they are located in the multiplex network. The formula represents the net amount of information transferred between nodes i and j. Indeed, the larger the information exchanged among i and j, the greater is G_{ij} and the closer are the nodes. On the contrary, when the nodes exchange a small amount of information, the value of G_{ij} is low, then the value of ξ_{ij} is big, and consequently, the nodes are distant.

In the multiplex network, the information spread by communicability is wider than the single-layer case. Indeed a node can exchange information through different channels, that is by other nodes of the same layer and by nodes belonging to different layers. This is the reason why we are interested in studying how layers exchange the information, or in other words, how distant nodes are in different layers. To stress the dependency of information flow with respect to the layers' connections through the inter-layer weight ω, we denote the distance ξ_{ij} as a function of ω:

$$\xi_{ij}(\omega) = G_{ii}(\omega) + G_{jj}(\omega) - 2G_{ij}(\omega). \quad (4)$$

3 Community detection on multiplex networks

In this section, we propose a method that allows to detect communities on multiplex networks. As a first step, we find the value of ω that minimizes the communicability distance between nodes. We denote this optimal value with ω^*. This assures a large information circulating in the multiplex. Then, using ω^*, we update the Estrada communicability for all nodes in the multiplex. In this way, we incorporate in the information exchanged between nodes the effect of the optimal inter-layer connections. Finally, using the communicability distance we perform a community detection layer by layer.

This procedure is based on the determination of a threshold ξ_α that is specific to each layer α. Let us focus our attention on this important point. The optimal partition results from an optimization problem whose objective function is based on the idea of cohesion between nodes and returns the optimal ξ_α. This threshold corresponds to the best possible partition under the best ω^*. This threshold ξ_α is, therefore, an endogenous element of the system and the communities, formed by the complicated interweaving of relations between different layers, emerge by the system in a natural way.

In the following, we describe in detail such a methodology.

3.1 Optimal inter-layer connections

The optimal inter-layer weight ω^* is obtained as a result of an optimization problem, where the objective function is a suitable map representing the distance between all pairs of nodes in a multiplex network. To this end, we define the average distance function for the node i, as follows:

$$\bar{\xi}_i(\omega) = \frac{1}{nh-1}\sum_{j\neq i}\xi_{ij}(\omega), \tag{5}$$

where nh is the total number of nodes in the multiplex.[3] By formula (5), we obtain the multiplex average distance:

$$\bar{\xi}(\omega) = \frac{1}{nh}\sum_{i}\bar{\xi}_i(\omega) = \frac{1}{nh\,(nh-1)}\sum_{i,j}\xi_{ij}(\omega). \tag{6}$$

Formula (6) expresses the multiplex average distance $\bar{\xi}(\omega)$ also as the average of the distances between all pairs of vertices in the multiplex.
We then define the multiplex distance $\Delta_M(\omega)$ as:

$$\Delta_M(\omega) = \sum_{i}\bar{\xi}_i(\omega) = nh\bar{\xi}(\omega). \tag{7}$$

By formula (7), this distance is proportional to the average distance for the whole network. We notice that this definition is in line with the results obtained for single-layer networks in Bartesaghi et al. (2022) in case of a partition made up of the entire network. In the Appendix A we report an alternative expression of the multiplex distance.
The following properties hold for the multiplex distance Δ_M (we refer the reader to the Appendix B for the proof):

Theorem 3.1 *Let $\Delta_M : [0,1] \to \mathbb{R}$ such that $\Delta_M(\omega) = nh\bar{\xi}(\omega)$. The following properties hold:*

1. *$\Delta_M(\omega)$ is positive.*
2. *$\Delta_M(\omega)$ belongs to $C^\infty(\mathbb{R})$.*
3. *$\Delta_M(\omega)$ has global minimum and maximum. The extreme point $\omega^* \in (0,1)$ satisfies the following equality*

$$nh\sum_{i}G'_{ii}(\omega^*) = \sum_{i,j}G'_{ij}(\omega^*),$$

where G' is the derivative of G.

To select the optimal weight ω^* between layers in the multiplex, we minimize the distance $\Delta_M(\omega)$.

[3] The network contains h layers with n nodes each. The average in formula (5) is computed dividing the numerator by $nh-1$ because it accounts for all the distances from i to all the remaining nodes.

3.2 Community detection

To assess the role of the inter-layer weights in the community structure, we perform a community detection on each layer extending to the multiplex case the procedure proposed by Bartesaghi et al. (2022).
Firstly, we compute the Estrada communicability matrix $\mathcal{G}(\omega^*)$ evaluated at the optimal value ω^*. In this way, we expand the information encoded in the communicability matrix, since we consider not only intra-layer paths but also inter-layer paths. Moreover, within this approach, it is possible to better assess the role played by each node in information spreading. Then, for all pairs of nodes i and j on each layer α, we calculate the optimal communicability distance $\xi_{ij,\alpha}(\omega^*)$ by means of formula (4). The latter expresses the optimal distance of nodes i and j in terms of Estrada communicability.

The community detection on each layer is performed by following the approach proposed in Bartesaghi et al. (2022). For each layer α, we consider members of the same community those nodes whose communicability distance is below a given threshold $\xi_\alpha \in [\xi_{\min,\alpha}, \xi_{\max,\alpha}]$, which is specific for each layer. The underlying idea is that the more two nodes in a layer are connected, the lower is their communicability distance. On the basis of threshold ξ_α, we construct the matrix $\mathbf{M}_\alpha(\omega^*) = [m_{ij,\alpha}(\omega^*)]$ of entries:

$$m_{ij,\alpha}\left(\omega^*\right) = \begin{cases} 1 & \text{if } \xi_{ij,\alpha}\left(\omega^*\right) \leq \xi_\alpha \\ 0 & \text{otherwise} \end{cases}$$

The best threshold ξ^*_α is obtained maximizing a quality function Q_α defined as follows:

$$Q_\alpha = \sum_{(i,j)\in E_\alpha}\gamma_{ij,\alpha}(\omega^*)x_{ij}, \tag{8}$$

where x_{ij} is a variable equal to 1 if two nodes are in the same community and 0 otherwise, and $\gamma_{ij,\alpha}(\omega^*)$ is:

$$\gamma_{ij,\alpha}\left(\omega^*\right) = \left(\bar{\xi}_{j,\alpha}(\omega^*) - \bar{\xi}_\alpha(\omega^*)\right) - \left(\xi_{ij,\alpha}(\omega^*) - \bar{\xi}_{i,\alpha}(\omega^*)\right), \tag{9}$$

with $\bar{\xi}_{i,\alpha}$ and $\bar{\xi}_\alpha$ defined in (5) and (6), respectively. Notice that $\gamma_{ij,\alpha}(\omega^*)$ is a measure of cohesion between nodes i and j [see Chang et al. (2016), Bartesaghi et al. (2022)]. Indeed, $\gamma_{ij,\alpha}(\omega^*) \geq 0$ yields $\xi_{ij,\alpha}(\omega^*) - \bar{\xi}_\alpha(\omega^*) \leq \bar{\xi}_{i,\alpha}(\omega^*) - \bar{\xi}_{i,\alpha}(\omega^*)$, i.e. intuitively, two nodes are cohesive if they are close to each other and, on average, they are both far away from the other nodes. Thus, by this procedure we group nodes that are close to each other, but far from the rest of the network, revealing the clusters of nodes that strongly communicate. Through the maximization of Q_α, we optimize the division in nodes clusters. We stress that this approach is in

line with those in Newman and Girvan (2004). Indeed, we do not choose a priori the number of communities, but the latter comes out from the maximization procedure. Concluding, we summarize the proposed methodology in the following steps:

1. First step: multiplex optimization
   (a) compute the multiplex communicability matrix $\mathcal{G}(\omega)$;
   (b) for all i and j compute the communicability distance ξ_{ij}, and their average values, based on the communicability matrix $\mathcal{G}(\omega)$;
   (c) compute the closed form of the multiplex distance $\Delta_M(\omega)$;
   (d) find the inter-layer weight ω^* such that the distance $\Delta_M(\omega)$ is minimized.
2. Second step: layer optimizations
   (a) compute the optimal multiplex communicability $\mathcal{G}(\omega^*)$;
   (b) for each layer iterate the following steps.
      (i) for all i and j of the same layer α compute the communicability distance $\xi_{ij,\alpha}(\omega^*)$ based on the communicability matrix $\mathcal{G}(\omega^*)$;
      (ii) calculate the layer cohesion measure Q_α;
      (iii) determine ξ^*_α, maximizing Q_α and find communities that satisfy the inequality $\xi_{ij,\alpha}(\omega^*) \leq \xi^*_\alpha$.

In Appendix C we report three toy examples to illustrate the role of the optimal inter-layer weight ω^* in the proposed community detection method.

4 Numerical section

We provide here an application of the proposed methodology to a multiplex network that considers different interconnected aspects of countries' behaviour during the coronavirus pandemic period, also known as the COVID-19 pandemic. In particular, we consider four layers that are the COVID-19 infections, the Stringency Index, the international trade, and the international air mobility. On each layer, we consider 51 nodes representing the countries.[4] To ensure that the constructed multiplex is node aligned, we consider only those countries for which there was data available for all layers.
We focus our analysis on the period April 1–June 30, 2020, that represented a timestamp characterized by both a high diffusion of the coronavirus disease and an implementation of heterogeneous response measures between countries, leading to many different outcomes in the international trade and air mobility. Unfortunately, in the previous period (January–March, 2020), also characterized by the diffusion of the disease and by the introduction of initial restrictions too, missing data were present at the worldwide level to assure a good calibration of the network.

4.1 Data sources and multiplex network

To construct the multiplex network used for the numerical application, we make use of four different data sources.
To build the two layers strictly related to COVID-19 diffusion, we collected from "Our World in Data", a project of Global Change Data Lab that involves University of Oxford, the new cases of COVID-19 disease and the Stringency Index values for each country on a daily basis.[5] As for the confirmed daily new cases of COVID-19 disease, the data available come from COVID-19 Data Repository by the Center for Systems Science and Engineering at Johns Hopkins University.
The second layer deals with the actions that governments around the world implement to stem the COVID-19 pandemic and it is based on the Government Response Stringency Index. The Stringency Index (SI) is a composite indicator of the government response strategy to the pandemic diffusion. This composite measure is a simple additive score of nine indicators evaluated on an ordinal scale and properly rescaled to vary from 0 to 100 [see Hale et al. (2021)]. Publicly available information on indicators of government response are collected. These indexes measure the level of restriction based on different policies, such as school closures and travel bans.[6]
The third layer deals with the international trade. For the analysed period, we collected the amount of trades between countries from the UN Comtrade, a repository of official international trade data, Nations (2021). The preliminary aggregation of data is based on the approach in Antonietti et al. (2022). Two countries are connected by an average value between their imports and exports if both exist, zero otherwise. An entry of the resulting matrix expresses the average value of trade exchanged between a a couple of countries.
The last layer handles the air mobility across countries. We collected data about the international air mobility from Schäfer et al. (2014). As a first step, we collect the international flights for the analysed period. Later, we associate to

[4] The list of countries and related codes is reported in the Appendix E. We notice that the list of countries does not contain France and Russia, which are between the largest economy in terms of trade. The reason lies in the lack of international trade data from Nations (2021) for these countries for the second quarter of 2020.

[5] Notice that data are also available on github at the following link: https://github.com/owid/covid-19-data/tree/master/public/data.

[6] The nine indicators are school closures, workplace closures, cancel public events, restrictions on gatherings, closure of public transport, public information campaigns, imposing to stay at home, restrictions on internal movement, international travel controls.

each country the sum of the international flights departing to and arriving from the airports in its territory, respectively. Therefore, in this case, the resulting matrix collects the total number of international flights between two countries.
Due to the heterogeneous nature of data and to assure comparability between layers, we compute for each layer the correlation coefficient between each couple of countries. In particular, on each layer, the network is constructed by following three steps:

- construct the correlation matrix on the empirical data;
- filter the non-significant correlations fixing a p-value threshold of 5%;
- ensure that weights lie in [0, 1] by the use of distance transformation proposed in Mantegna (1999).

For the COVID-19 and Stringency Index layers, the correlation coefficients have been computed between the time series of the observed phenomena for each couple of countries. Therefore, the generic element of the correlation matrix of each layer gives a measure of linear dependence between two countries in terms of COVID-19 infections and containment measures.
For the remaining layers, each element of the correlation matrix represents the level of similarity (or dissimilarity) between two countries in terms of exposure to all other countries with respect to either trade or international air mobility data. Indeed, given the matrix collecting the empirical average trade value, the associated correlation matrix is constructed by calculating the correlation between the average trade value that two countries exchange with the rest of the world. Similarly, the elements of the correlation matrix of the international flights express the correlation between the number of international flights that connects two countries with the rest of the world.
For each layer, the correlation matrix is then filtered by setting to zero the entries whose p-values are less than a threshold fixed to 5% and keeping the significant correlations.
We define $\rho_{ij,\alpha}$ as the significant correlation coefficients between countries i and j on each layer α. To assure that the weights of links range in the interval [0, 1], a meaningful solution has been proposed in Mantegna (1999) [and adapted in Giudici et al. (2020)] based on distances

$$d_{ij,\alpha} = 1 - \frac{1}{2}\sqrt{2\left(1 - \rho_{ij,\alpha}\right)}.$$

Hence, we construct four distinct single-layer networks G_α reported in Figs. 13 and 14 in the Appendix E.

A link between nodes i and j exists in the network G_α only if a significant correlation exists between countries i and j in the layer α. The weighted adjacency matrix $\mathbf{W}_\alpha$ has entries equal to

$$w_{ij,\alpha} = \begin{cases} d_{ij,\alpha} & \text{if } d_{ij,\alpha} > 0 \\ 0 & \text{otherwise} \end{cases}.$$

Given the strict relations between the four dynamics involved, we construct a multiplex network based on a supradjacency matrix $\mathcal{W}$ built as described in the methodological section. In particular, we consider $\mathbf{W}_L$ the block matrix of the adjacency matrices $\mathbf{W}_\alpha$, $\alpha = 1, \ldots, 4$ of the layers and the block matrix $\mathbf{C}_{LL}$ of all the inter-layer connections based on ω that expresses the inter-layer weight between nodes.

4.2 Preliminary analysis

We start considering separately the four layers and we display in Table 1 some topological features. It is noteworthy that for the first three layers, the density is around 80% that means that the correlation coefficients are significant for a consistent number of pairs. For the same layers, also the weighted clustering coefficient, computed here using Barrat et al. (2004), shows a high value due to both the presence of several triangles and a high average correlations.
It is also noticeable that the Stringency Index and international trade data are characterized by a high average correlation due to similarities between countries at the international level. Probably this is motivated by a common reaction to the pandemic situation and by a similar impact on trades related to the restrictions in force. More heterogeneous patterns have been instead observed in terms of COVID-19 infections and mobility. Finally, it is interesting that, although the air mobility network has a lower density, a clustering coefficient similar to the other layers is observed. Indeed, despite on average each country has a lower number of connections, we have that neighbours of a country are usually connected forming a triangle.

4.2.1 COVID-19 infections

We focus here on the first layer of the multiplex network. It is interesting to notice that the network based on COVID-19 cases (see top network in Fig. 13) is characterized by a dense group, with high average weights, involving mainly European countries and a second group including Eurasian, Asian, Central American, and African countries. The two groups are connected by links with very low distances associated to negative correlation coefficients. This is mainly explained by the different diffusion in these two groups of the pandemic infections during the first wave. As shown in Al-Salem et al. (2021), Italy, Belgium, France, Germany, Great Britain, Netherlands, and Spain showed the highest number of cases in Europe in the analysed period with very high peaks of infections and deaths in April 2020. These countries show indeed a very high correlation with each other. The second

Table 1 Global network indicators of each layer

Layer	Size	Density	Average weight	Average degree	Clustering
COVID-19	1029	0.81	0.28	40.35	0.90
Stringency Index	1111	0.87	0.51	43.57	0.94
International trade	1026	0.80	0.43	40.23	0.87
International mobility	640	0.50	0.28	25.09	0.78

group is instead represented by countries that were affected lately by the diffusion. It is also interesting to note the different behaviour of Sweden that seems not so close to the other European countries, providing a negative correlation. Sweden indeed has been characterized by a different national strategy with respect to the other countries and it has represented an outlier with cases and deaths increasing more rapidly than in its Nordic neighbours in the second wave of COVID-19 [see, e.g. Claeson and Hanson (2021) and Gordon et al. (2021)]. It is also noticeable that the behaviour of Japan, USA, and Israel are connected to the dense European group.

4.2.2 Stringency Index

The second network in Fig. 13 is based on the values of the Stringency Index and, therefore, it is related to alternative strategies introduced by governments in the analysed period. First of all, we observe a higher average distance with respect to the other networks. This means that the correlation between countries is significantly higher in this case.[7] Although every country's lockdown is different and a wide range of measures have been adopted by national governments, a high correlation between Stringency Index is observed on average. This result shows on average homogeneous indices between countries, although characterized by combinations of different restriction policies. Also, Sweden shows a positive correlation with other countries, but provides the lowest average value in Europe. This is mainly motivated by the fact that the country had relaxed requirement during the first pandemic wave. For instance, Sweden maintained an open border in the first half of 2020 within the EU and beyond has imposed no quarantine requirements for arrivals (Gordon et al. 2021). In addition to an open border, Sweden minimized its government-mandated social distancing measures and placed a greater reliance on the voluntary behaviours of Swedish residents to comply with national health advisories [see, e.g. Paterlini (2020) and Ludvigsson (2020)]. Specific patterns can be observed also for some American countries (as for instance, Guatemala), characterized by a initial lower incidence of the virus and by low level of restrictions in that period.

4.2.3 International trade

The third layer is related to the volume of trades between countries (see the first network in Fig. 14). This network shows a high density (equal to 0.80) because of a high presence of significant correlations. Moreover, all the correlation coefficients are positive showing similar economic dynamics between countries in the period. This evidence can be justified by a common reduction trend observed between countries. Indeed, worldwide merchandise trade flows decreased significantly in 2020, as COVID-19 disrupted economic activity across the globe. Various pandemic-related factors shaped international trade flows. Specifically, COVID-19 incidence and lockdown restrictions affected the volume of imported and exported goods. For instance, Liu et al. (2022) find that government measures to curb economic activities had a larger impact on China's imports than the direct health and behavioural effects of the pandemic itself.

4.2.4 International air mobility

The last layer focuses on the air mobility between countries (see the second network in Fig. 14). In this case, a lower density is observed because of a high presence of non-significant correlations. The network is indeed heavily affected by the different actions in terms of travelling restriction that Governments put in place to fight the pandemic as well as by the effects of one of the worst crisis in the aviation industry. As expected, geographic proximity has a relevant influence on the correlation based on the number of flights. Additionally, it should be considered that although passenger flights were cancelled, cargo flight were allowed during the analysed period. However, the cargo capacity has been also reduced because of rising costs. A preliminary inspection of data shows values of correlation higher than 0.5 in two different situations. On the one hand, high correlation occurs between countries as China, Netherlands, Denmark, and Belgium, which are involved in intense economic activities, and this is reflected also by the number of cargo flights present in the used data.

[7] The average correlation in the network based on COVID-19 cases is 0.05. It is equal to 0.51 for the Stringency Index, 0.45 for the international trade, and 0.30 for the air mobility.

Table 2 Clusters detected by applying the proposed methodology on multiplex network and the single-layer, respectively

	Multiplex ($\omega = \omega^*$)			Single-layer ($\omega = 0$)		
	ξ^*_α	Q_α	N. of communities	ξ^*_α	Q_α	N. of communities
COVID-19	1.391	80.14	10	1.385	79.26	12
Stringency Index	1.397	73.45	7	1.395	73.46	22
Int. trade	1.398	76.39	5	1.395	76.65	5
Int. mobility	1.391	80.62	11	1.385	80.89	14

On the other hand, high values of correlation can be observed among countries characterized by a low level of Stringency Index, such as Sweden and Romania, that allowed the air traffic more than in other countries. These results confirm the strong relations that mutually connect the international trade and the international mobility with the containment measures.

4.3 Results

The community detection approach has been initially applied separately on each network G_α, i.e, assuming $\omega = 0$. In this way, we analyse the mesoscale structure of each layer without being affected by the topological structure of the other layers. Then, the proposed methodology was applied according to the steps described in Sect. 3 focusing on the whole multiplex network and considering the optimal weight ω^*.

First, ω^* was computed by formula (7), then the community detection method provided in Sect. 3.2 was applied on each layer considering the reciprocal influence between layers due to the presence of ω^*. The aim is to emphasize possible differences in the mesoscale structures with respect to the single-layer case and to highlight the advantages of a multiplex framework in terms of influence. The optimal inter-layer weight ω^* expresses the optimal connection (in terms of communicability) between different and possibly correlated slices of a complex system, capturing here various aspects of the coronavirus pandemic. It is worth trying to understand what is the influence of one layer on the others and on the entire multiplex. In our case, the optimal inter-layer weight ω^* that ensures the minimum multiplex distance between nodes in the multiplex is equal to 0.7. The high value of ω^* indicates a high average flow of information[8] among a node and its replicas and, therefore, denoting a strong influence between layers.

Main global results of the community detection method are presented in Table 2 and Fig. 2 shows the value of the multiplex distance $\Delta_M(\omega)$ varying ω. A first interesting evidence is that the proposed optimization assured a low optimal distance in the multiplex analysed. Indeed, in the single-layer case, $\Delta_M(\omega)$ is equal to 290.4, which is higher than $\Delta_M(\omega^*)$ that is equal to 289.9. Indeed, we have a higher optimal threshold in each layer when the multiplex is considered as a whole. This implies a lower number of communities, which benefit from a higher cohesion.

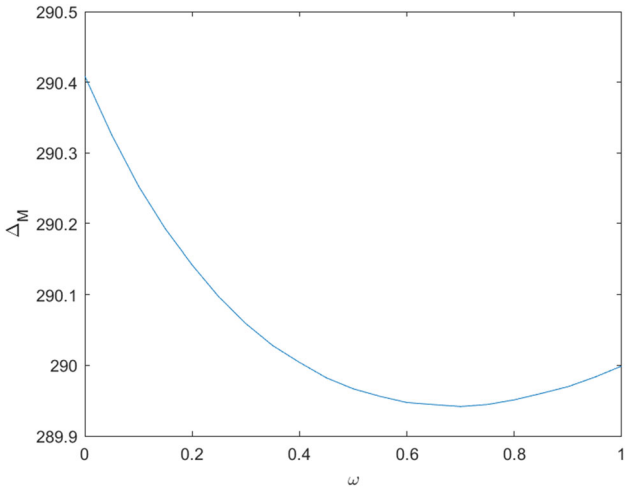

Fig. 2 Multiplex distance varying ω

4.3.1 COVID-19 infections

Focusing on the clusters obtained with the proposed methodology for the COVID-19 multiplex network, we observe two relevant communities in Fig. 3b. The largest one collects together a major part of Europe, the UK, the USA, and Australia. This result could be explained by the evidence of a similar pattern of all these countries in terms of disease diffusion in the analysed period. The pattern of the pandemic has indeed varied across countries, but, for instance, a common feature across Europe has been the presence of a first wave occurring in the spring of 2020. This wave was followed by a consistent reduction in the spread of the virus in the summer and a resumption of the epidemic activity in 2020 with the second and/or third waves [see, e.g. Remuzzi and Remuzzi (2021)]. In the first phase, Italy was the original epicentre of the COVID-19 pandemic in Europe, with a subsequent spread in Western and Northern Europe [see, e.g. Villani et al. (2021)]. The UK, Spain, Germany, countries of Benelux Union, Denmark, Norway, and Finland are indeed characterized by similar levels of cases in the period and

[8] We remind that the communicability distance can be seen as an information flow, see Estrada (2012a).

belong to the same community (see community 1 in Fig. 3b). Eastern Europe was instead less affected by the virus in the first phase. For instance, Slovakia (not included in community 1, see Fig. 3b) was less affected by the COVID-19 virus in the first wave and has shown an increase in cases, and consequently in deaths, during the second phase [see Villani et al. (2021)]. Sweden is not present in this group, being characterized by an anomalous behaviour in that period with respect to other Nordic regions (Claeson and Hanson 2021). A second large community includes Asian, Eurasian, Central American and African countries, hence characterized by a lower incidence in the fist wave.

On the contrary, the mesoscale structure in case of independent layers, i.e. setting $\omega = 0$, is quite different (see Fig. 3a). It shows two large clusters based on the COVID-19 spreading time: a first cluster made by countries characterized by a high level of contagion and a second one containing countries that did not have a high rate of infection during the first wave. It is noticeable that in the third community including Israel and the USA, COVID-19 confirmed daily case correlation was around 0.7. These two countries belong instead to community 1 when the multiplex network is considered. This different grouping assures a higher cohesion.

In particular, two effects of the inter-layer weight ω^* on the community detection can be noticed. Indeed, the community 2 (the light blue one in Fig. 3b) has been formed through two different actions. With respect to the single-layer case, some countries migrate to the first community and the third community (the pink one in Fig. 3a) is fully incorporated. The presence of ω^* indeed favours the aggregation of countries with similar behaviour in terms of daily confirmed COVID-19 cases looking at the entire multiplex.

4.3.2 Stringency index

In the case of community detection based on independent layers, the Stringency Index layer presents a fragmented structure with 22 communities (see Fig. 4a). Indeed, the pandemic has varied in different countries or regions due to differences both in the capacity of countries to adapt their health system to the COVID-19 epidemic and in governmental policy responses.

Certainly, governments around the globe have been taking a wide range of social control measures in response to the COVID-19 outbreak with different degrees and intensities. For instance, as shown in Ma et al. (2021), countries have been characterized by a different first day of response (i.e. first day with Stringency Index higher than zero) to the pandemic situation. Few Asian countries reacted in the first half of January, while European countries, USA, and Canada introduced the first measures between the second half of January and the month of February. Other European countries (as Sweden and several states of Eastern Europe), Brazil, and Mexico introduced the first measures only at the end of February and during the month of March. Finally, the rest of the world (mainly Kazakistan, Bolivia, and several African countries) initiated a response after 11th of March 2020, the day World Health Organization (WHO) declared COVID-19 as a global pandemic.

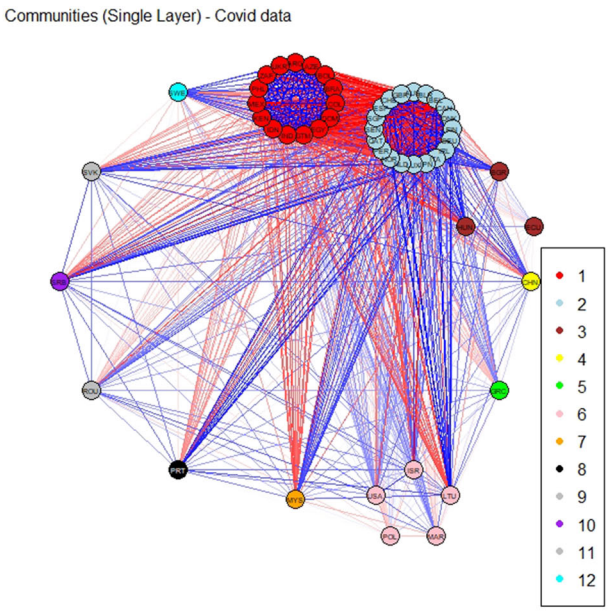

(a) Community detection on COVID-19 layer ($\omega = 0$).

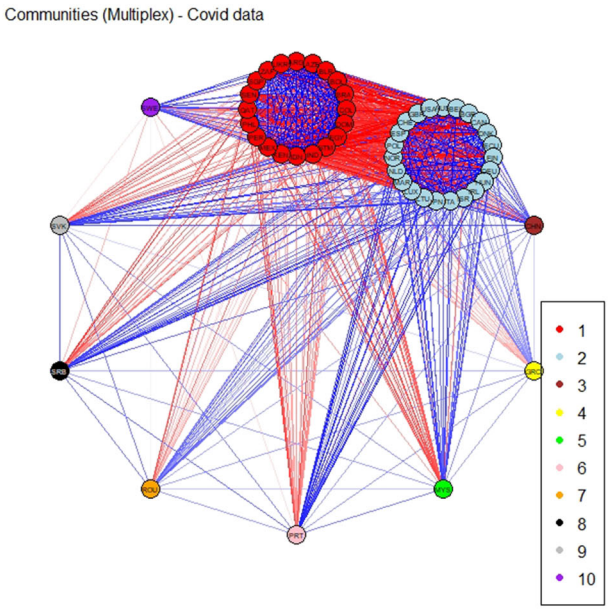

(b) Community detection on COVID-19 layer ($\omega = \omega^*$)

Fig. 3 Impact of ω on the community detection of COVID-19 network

When the community detection is applied using ω^*, a lower heterogeneity was observed. Indeed, on the Stringency Index network, seven communities were identified, among them a large community and two smaller ones (see Fig. 4b). This result shows the aggregating effect of the optimal inter-layer weight. It can be explained noticing that the connection with other layers reduces the heterogeneity in the layer.
Additionally, data focus on the second quarter of 2020 and, therefore, clusters' composition is affected by the average level of restrictions in the period. In particular, countries characterized by very high level of Stringency Index are on average in community 1 (see Fig. 4b). In this group, we find mainly countries that upgraded the containment measures to a very high level and kept these rules in force for a long period. In particular, Italy, Central European countries (e.g. Netherlands, Luxembourg, Germany, Denmark), Portugal, Israel, and India are all characterized by values of the Stringency Index that belong to the top quartiles of the SI distribution in the analysis made by Ma et al. (2021). The same community includes also countries that maintained moderate levels of the Stringency Index such as the USA, Canada, Australia, and Japan.

4.3.3 International trade

According to the layer based on volumes of trade at the international level, we notice a large community including Asia-Pacific and American countries and a large European cluster. A peculiar case is represented by Germany that acts as a isolated node. This is mainly due to the significant reduction in the volume of trades that characterized this country in the analysed period. Indeed, based on the Economic Research of the Federal Reserve Bank, the volume of exports in Germany reduced roughly 1/4 in the second quarter of 2020.[9] This behaviour represents a novel result with respect to other studies in the literature that focused on the first semester of 2020 [see, e.g. Antonietti et al. (2022)].
Furthermore, the pattern of trade during the pandemic period strengthened the geographical relationships between countries. In particular, in Europe there are preferential channels of internal exchanges, whereas, outside Europe, most communication channels seem to be polarized around the exchanges between American and Asian countries. The health crisis indeed led to confused and non-cooperative responses, characterized by more or less direct and formal export restrictions, including within the European Union (EU) [see Baldwin and Evenett (2020) and Bown (2020)]. In particular, as described in Evenett et al. (2022), countries responded to the COVID-19 pandemic with various combinations of export controls and import liberalization measures. Some countries acted on both sides, creating long-term changes in their pre-COVID-19 trade policy structures for the food and medical sectors. Other countries ruled only on one side, either restricting trade or liberalizing it. Although EU Member States reacted with a certain level of heterogene-

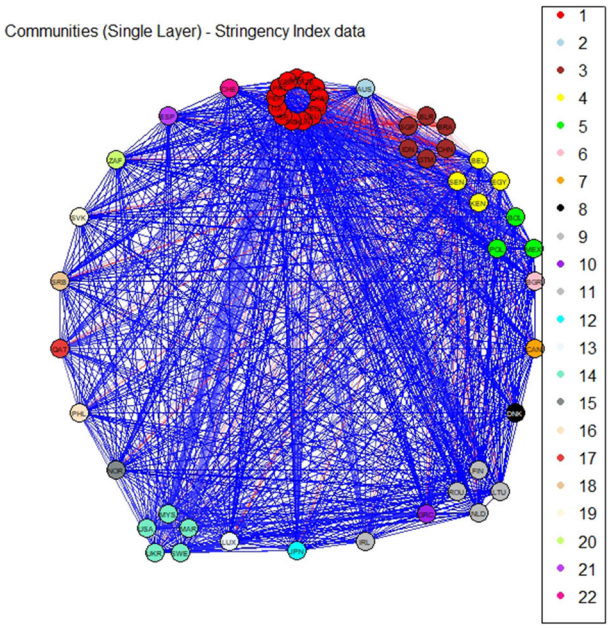

(a) Community detection on Stringency Index layer ($\omega = 0$).

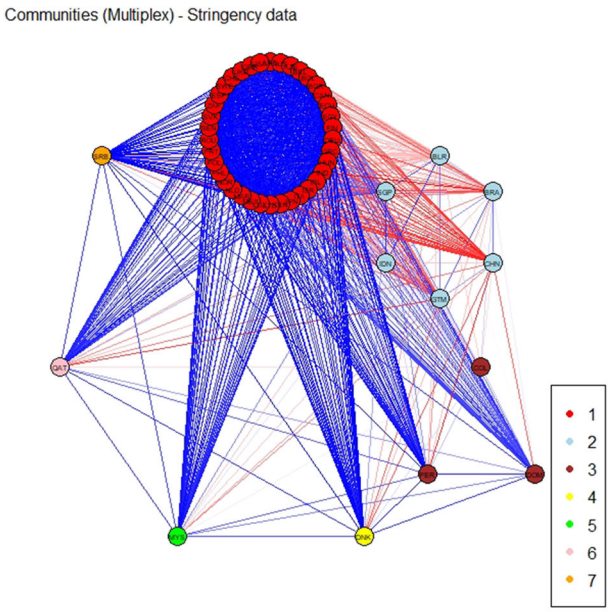

(b) Community detection on Stringency Index layer ($\omega = \omega^*$)

Fig. 4 Impact of ω on the community detection of Stringency Index network

[9] See online database containing Federal Reserve Economic Data (FRED).

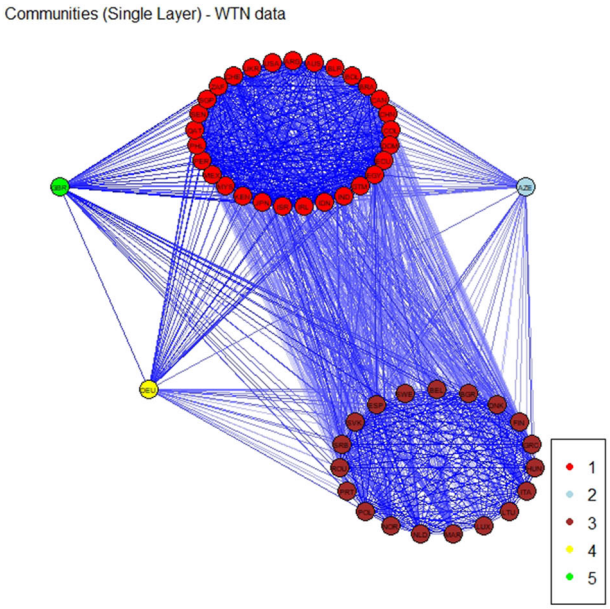

(a) Community detection on international trade layer ($\omega = 0$).

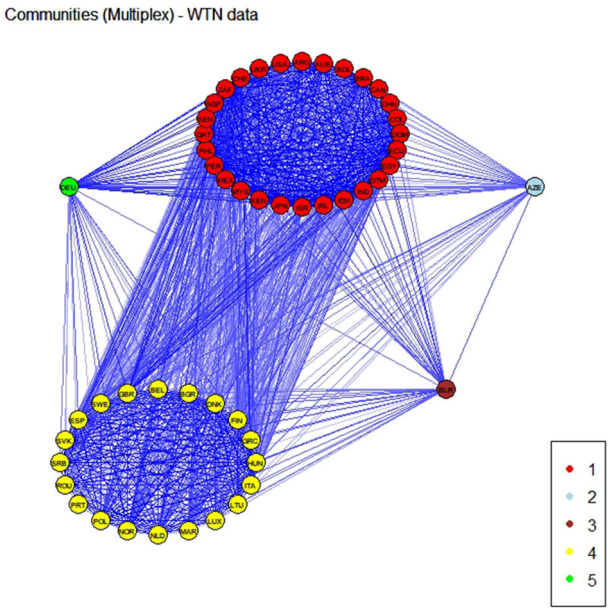

(b) Community detection on international trade layer ($\omega = \omega^*$)

Fig. 5 Impact of ω on the community detection of Stringency Index network

ity, a common commercial effect is noticeable also due to the role played by the European Commission. This behaviour can motivate the composition of community 2 in Fig. 5.

Fig. 5 also highlights that the World Trade Network is characterized by a strong mesoscale structure. Indeed, this characteristic is evident in the stability of the communities composition with respect to other studies involving volumes of trade and based on other time periods (see Antonietti et al. (2022)).

The stability of the mesoscale structure is also explained by the fact that aggregated data does not allow to catch peculiar patterns regarding specific sectors (such as, for example, pharmaceutical industry). Additionally, the analysis focuses only on the first period of the COVID-19 pandemic situation and, reasonably, the main impacts are not fully reflected on the trade volumes.

4.3.4 International air mobility

Also for the international air mobility network, we can observe in Fig. 6 a fragmented structure, in which two large clusters emerge. In particular, when the optimal inter-layer weight is considered, the two clusters are well balanced in terms of number of components, while, considering the single independent layers, a huge community 1 is observed. Focusing on results in the multiplex approach, a first cluster, composed by Asia-Pacific and South American countries, appears. A second cluster is characterized by the presence of several European states. This result reflects an opposite behaviour during the COVID-19 pandemic.

As stressed before, in case of the independent layers, a large community 1 is present (see Fig. 6a), but two internal subgroups can be identified. On the one hand, there are countries characterized by a low number of international flights even before the COVID-19 disease, such as Egypt and Peru. On the other hand, we observe a group of nodes that drastically reduced the air mobility during the first wave of COVID-19 pandemic, for example China and Australia. The second cluster, consisting of European countries, also includes both countries that have temporarily reduced the number of flights and those that have not, such as Sweden.

The distinction between countries involved in the COVID-19 pandemic is further emphasized in the multiplex approach, i.e. $\omega = \omega^*$. In the first cluster, we have countries characterized by a low contagion intensity during the period, while the second main cluster consists of countries that were struggling with a pandemic scenario at the same period. Once again, the methodology shows that when the community partition is conducted considering the influence of all other layers (daily COVID-19 cases, Stringency Index, international trade), the number of clusters decreases aggregating countries that have a similar pattern.

4.3.5 Structural similarities between layers

To detect possible structural similarities, we compare the clusters obtained on the four layers. Several approaches for comparing communities have been proposed in the literature [for a review we refer, for instance, to Danon et al. (2005)].

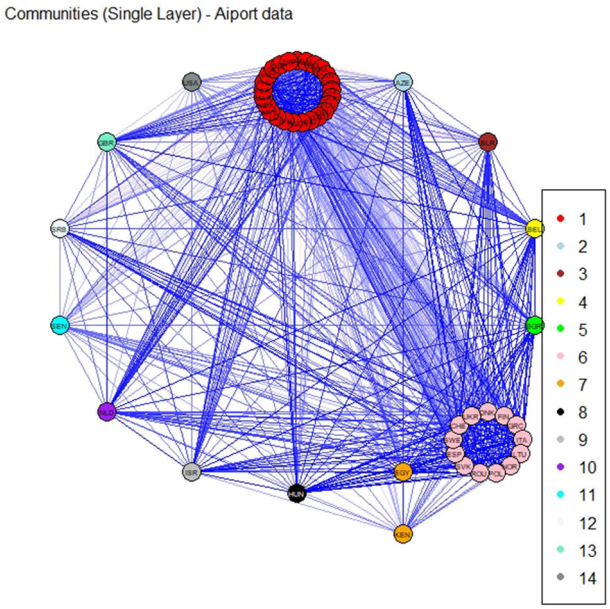

(a) Community detection on international mobility layer ($\omega = 0$).

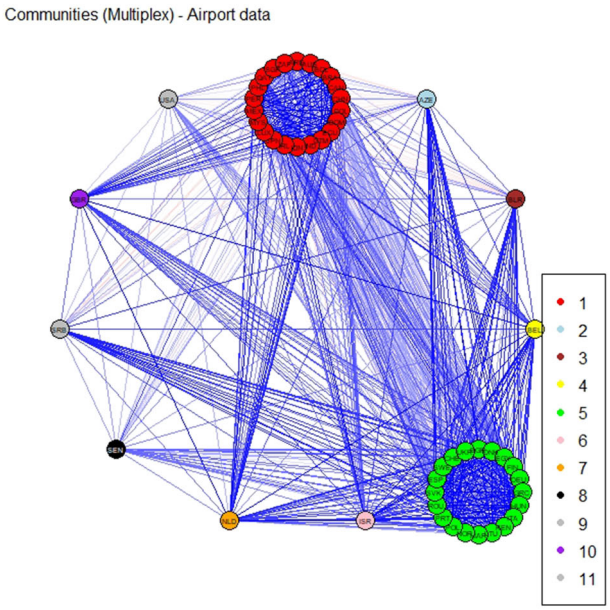

(b) Community detection on international mobility layer ($\omega = \omega^*$)

Fig. 6 Impact of ω on the community detection of international mobility network

Here, we apply the normalized mutual information index, a discriminatory measure based on similarity between partitions [see Amelio and Pizzuti (2015); Lancichinetti et al. (2008)]. The measure ranges in the interval [0, 1] assuming the maximum value when identical partitions are detected. The results are reported in Tables 3 and 4, for separate layers and multiplex analyses, respectively.

As regards the case $\omega = 0$, we notice higher levels of similarity between air mobility and the other layers. This result is not surprising. Air mobility represents one of the main ways in which goods and people and, therefore, the epidemic, move from one country to another. Additionally, a strict connection with the Stringency Index exists. However, we do not observe a level of the index equal to 1 for this pair of layers, since in the Stringency Index several other containment measures are taken into account.

According to the community detection based on the optimal value ω^*, we observe an average increase of the similarities between layers due to the fact that the optimal value induces a common effect between layers. In particular, the COVID-19 mesoscale structure is strictly connected to the other layers. The similarity with the Stringency Index and the air mobility indicates that common levels of restrictions and observed reductions in the mobility between countries can be associated with similar effects in terms of infections. Finally, we notice also a high value of the index between mobility and trade, due to the fact that restrictions led to favour geographical proximity both in trades and mobility.

5 Conclusions

In this paper, we assess the relationship between various facets of the pandemic. To this end, we build a complex structure incorporating COVID-19 infections, containment measures, volume of trades and air international mobility during the second quarter of 2020.

The analysis of the mutually relationships between these different frameworks has been performed through a mathematical approach based on a multiplex network with four layers. We highlight the interdependence through an interlayer intensity parameter, optimally tuned in a way that minimizes the distance of the entire multiplex. Then, on the multiplex network we perform a community detection on each layer based on the Estrada communicability distance.

The proposed approach is meaningful to enhance possible similar behaviours of countries in reaction to a worldwide pandemic situation, involving simultaneously different aspects of human life. Indeed, we take into account different contexts (social, economic, healthcare and mobility) that have been directly or indirectly affected by the pandemic situation.

Results show that the multiplex approach catches a communication between layers higher than considering layers separately, allowing to refine the communities obtained. Indeed, we observe that the clusters are characterized by a higher cohesion, due to a lower internal distance. Focusing on COVID-19 layer, two big clusters emerge, characterized by

Table 3 Normalized mutual information index matrix for communities detected assuming $\omega = 0$

	COVID-19	Stringency Index	International trade	International mobility
COVID-19	1	0.36	0.19	0.37
Stringency Index	0.36	1	0.17	0.39
International trade	0.19	0.17	1	0.32
International mobility	0.37	0.39	0.32	1

Table 4 Normalized mutual information index matrix for communities detected assuming $\omega = \omega^*$

	COVID-19	Stringency Index	International trade	International mobility
COVID-19	1	0.32	0.30	0.32
Stringency Index	0.32	1	0.21	0.24
International trade	0.30	0.21	1	0.40
International mobility	0.32	0.24	0.40	1

a strong presence and a low occurrence of infections, respectively. A similar dichotomy is observed in the Stringency Index layer, allowing to highlight similarities in the policy-maker decisions worldwide. Considering international trade layer, European, Pacific and North European clusters have been obtained. In this case, a persistence of the mesoscale structure is confirmed with a strengthening of the geographical relationships between countries. In the international air mobility layer two distinct behaviours emerge: a cluster with countries marginally touched by the contagion, and a second cluster of countries strongly involved in the pandemic scenario. As expected, similarities in the countries' behaviour between this and the other layers are remarkable, confirming that a complex quantitative approach is appropriate to effectively study this type of phenomena.

This proposal provides a contribution to the field of community detection in multiplex networks. However, further research in the application of community detection holds great promise in unveiling the intricate structure of interconnected systems, enabling to identify cohesive groups and understand their functional roles across different layers. By developing advanced algorithms and methodologies, future studies can delve deeper into the dynamics of multilayer communities, uncovering their evolution over time and shedding light on the underlying mechanisms that drive their formation and resilience.

Acknowledgements Research by Rosanna Grassi and Giorgio Rizzini has been financially supported by Fondo di Ateneo Quota Competitiva 2021, University of Milano - Bicocca.
We would like to thank the anonymous reviewers for their careful reading and their insightful suggestions.

Author Contributions Conceptualization: GPC, RG and GR. Methodology: RG and GR. Data curation: GPC and GR. Formal analysis and investigation: GPC and GR. Writing - review and editing: GPC, RG and GR. Writing-original draft preparation: GPC, RG and GR. Funding acquisition: RG.

Funding The authors have no relevant financial or non-financial interests to disclose.

Data Availability The datasets generated and/or analysed during the current study are available from the corresponding author upon reasonable request.

Declarations

Conflict of interest The authors have no competing interests to declare.

Ethical approval Not applicable.

Consent to participate Not applicable.

Consent for publication Not applicable.

Appendix A. Multiplex distance and cohesion measure

We show that the multiplex distance $\Delta_M(\omega)$ can be rewritten as the sum of γ_{ij}, where $\gamma_{ij} = \left(\bar{\xi}_j - \bar{\xi}\right) - \left(\xi_{ij} - \bar{\xi}_i\right)$ is a measure of cohesion between nodes i and j [see Chang et al. (2016)]. Specifically, $\left(\xi_{ij} - \bar{\xi}_i\right)$ represents the relative distance between nodes i and j and $\left(\bar{\xi}_j - \bar{\xi}\right)$ represents the relative distance from a random node to the node j. Two nodes are more cohesive if they are (relatively) more close each other than they are to any other node in the network. Indeed:

$$\begin{aligned}\Delta_M(\omega) &= nh\bar{\xi} \\ &= 2\,(nh)^2\,\bar{\xi} - 2\,(nh)^2\,\bar{\xi} + nh\bar{\xi} \\ &= (nh)^2\,\bar{\xi} - (nh)\,(nh-1)\,\bar{\xi} + (nh)^2\,\bar{\xi} - (nh)^2\,\bar{\xi}.\end{aligned}$$

Recalling formulas (5) and (6), i.e. $\sum_i \bar{\xi}_i = (nh)\bar{\xi}$ and $\sum_{i,j} \xi_{ij} = nh\,(nh-1)\bar{\xi}$, we have:

$$\begin{aligned}\Delta_M(\omega) &= nh\left(\sum_j \bar{\xi}_j\right) - \sum_{i,j}\xi_{ij} + nh\left(\sum_i \bar{\xi}_i\right) - (nh)\,(nh)\,\bar{\xi}\\ &= \sum_i\left(\sum_j \bar{\xi}_j\right) - \sum_{i,j}\xi_{ij} + \sum_j\left(\sum_i \bar{\xi}_i\right) - \sum_{i,j}\bar{\xi}\\ &= \sum_{i,j}\bar{\xi}_j - \sum_{i,j}\bar{\xi} - \sum_{i,j}\xi_{i,j} + \sum_{i,j}\bar{\xi}_i\\ &= \sum_{i,j}\left((\bar{\xi}_j - \bar{\xi}) - (\xi_{ij} - \bar{\xi}_i)\right) = \sum_{i,j}\gamma_{ij}.\end{aligned}$$

Appendix B. Proof of Theorem 3.1

We first recall the following results concerning the series of complex-valued functions [see Rudin et al. (1964), Ch. 7], that obviously also hold for real-valued ones:

Theorem B.1 (Test for uniform convergence) *Let $\{f_n\}$ be a sequence of complex-valued continuous functions on a set E in a metric space and f a complex-valued function defined in E. Suppose $|f_n(x)| \le M_n$, $\forall x \in E$. Then $\sum f_n$ converges uniformly on E if $\sum M_n$ converges.*

Theorem B.2 *Let $\{f_n\}$ be a sequence of complex-valued continuous functions on E and f a complex-valued function defined in E. If $\{f_n\}$ converges uniformly on E to the function f, then f is continuous on E.*

Theorem B.3 *Let $\{f_n\}$ be a sequence of complex-valued differentiable functions on $[a,b]$ such that $\{f_n(x_0)\}$ converges for some point x_0 on $[a,b]$. If $\{f_n'\}$ converges uniformly on $[a,b]$, then $\{f_n\}$ converges uniformly on $[a,b]$ to a function f and $\lim_{n\to\infty} f_n'(x) = f'(x)$, $x \in [a,b]$.*

Theorems (B.2) and (B.3) can be easily extended to the series of functions, being a series of functions uniformly convergent if the sequence of partial sums is.

Proof of Theorem 1

1. $\Delta_M(\omega)$ is positive being the product of nh and the average distance $\bar{\xi}$.
2. To prove the continuity and differentiation of $\Delta_M(\omega)$, by linearity it is enough to show that G_{ij} is a continuous and differentiable function. Indeed, by formula (7):

$$\begin{aligned}\Delta_M(\omega) &= nh\bar{\xi}(\omega)\\ &= \frac{nh}{nh(nh-1)}\sum_{i,j}\xi_{ij}(\omega)\\ &= \frac{1}{(nh-1)}\sum_{i,j}\xi_{ij}(\omega),\end{aligned}$$

with $\xi_{ij} = G_{ii} + G_{jj} - 2G_{ij}$, where $G_{ij} = \sum_{k=0}^{\infty}\frac{[\mathcal{A}^k]_{ij}}{k!}$. The ij-entries $[\mathcal{A}^k]_{ij}$ are monotonic polynomial functions of at most degree k in the variable ω; we denote these functions by $P_k(\omega)_{ij}$, then $\sum_{k=0}^{\infty}\frac{P_k(\omega)_{ij}}{k!}$ is a series of continuous functions.
As $P_k(\omega)_{ij}$ are monotonic functions in $[0,1]$, it is immediate to see that:

$$\frac{P_k(\omega)_{ij}}{k!} \le \frac{P_k(1)_{ij}}{k!} \quad \forall k > 0, \quad \forall i, j \in V,$$

and the series $\sum_{k=0}^{\infty}\frac{P_k(1)_{ij}}{k!}$ is convergent. Then, by Theorem (B.1), $\sum_{k=0}^{\infty}\frac{P_k(\omega)_{ij}}{k!}$ uniformly converges, and, by Theorem (B.2), G_{ij} is a continuous function.
The ij-entries $[\mathcal{A}^k]_{ij}$ are differentiable, with derivatives that are polynomial functions of at most degree $k-1$ in the variable ω. Moreover, the series of derivatives uniformly converges, then by Theorem (B.3), the sum of the series is G_{ij}'. This proves that G_{ij} is differentiable in $[0,1]$. By similar arguments, we prove that G_{ij} belongs to $C^{\infty}(\mathbb{R})$.
3. By Weierstrass theorem, $\Delta_M(\omega)$ has global minimum and maximum. The first derivative can be written as

$$\begin{aligned}\Delta_M'(\omega) &= \frac{1}{nh-1}\sum_{i,j}\xi_{ij}'(\omega)\\ &= \frac{1}{nh-1}\sum_{i,j}\left(G_{ii}' + G_{jj}' - 2G_{ij}'\right)\\ &= \frac{1}{nh-1}\left(\sum_{i,j}G_{ii}' + \sum_{i,j}G_{jj}' - 2\sum_{i,j}G_{ij}'\right)\\ &= \frac{1}{nh-1}\left(nh\sum_{i}G_{ii}' + nh\sum_{j}G_{jj}' - 2\sum_{\mathrm{i,j}}G_{ij}'\right)\\ &= \frac{1}{nh-1}\left(nh\sum_{i}G_{ii}' + nh\sum_{i}G_{ii}' - 2\sum_{i,j}G_{ij}'\right)\\ &= \frac{2nh}{nh-1}\sum_{i}G_{ii}' - \frac{2}{nh-1}\sum_{i,j}G_{ij}'.\end{aligned}$$

At the extreme points $\omega^* \in (0,1)$, $\Delta_M'(\omega^*) = 0$, then

$$\frac{2nh}{nh-1}\sum_{i}G_{ii}' - \frac{2}{nh-1}\sum_{i,j}G_{ij}' = 0$$

that yields

$$nh\sum_{i}G_{ii}' = \sum_{i,j}G_{ij}'.$$

Table 5 Supradjacency matrices for networks M_A, M_B, M_C

Multiplex network M_A

$$\mathbf{W}_1 = \begin{bmatrix} 0 & 0.35 & 0.35 & 0 & 0 & 0 & 0 \\ 0.35 & 0 & 0.35 & 0.05 & 0 & 0 & 0 \\ 0.35 & 0.35 & 0 & 0 & 0 & 0 & 0 \\ 0 & 0.05 & 0 & 0 & 0.5 & 0.5 & 0 \\ 0 & 0 & 0 & 0.5 & 0 & 0.5 & 0.5 \\ 0 & 0 & 0 & 0.5 & 0.5 & 0 & 0.5 \\ 0 & 0 & 0 & 0 & 0.5 & 0.5 & 0 \end{bmatrix} \quad \mathbf{W}_2 = \begin{bmatrix} 0 & 0.7 & 0.7 & 0.7 & 0.7 & 0.7 & 0.7 \\ 0.7 & 0 & 0.7 & 0.7 & 0.7 & 0.7 & 0.7 \\ 0.7 & 0.7 & 0 & 0.7 & 0.7 & 0.7 & 0.7 \\ 0.7 & 0.7 & 0.7 & 0 & 0.7 & 0.7 & 0.7 \\ 0.7 & 0.7 & 0.7 & 0.7 & 0 & 1 & 1 \\ 0.7 & 0.7 & 0.7 & 0.7 & 1 & 0 & 1 \\ 0.7 & 0.7 & 0.7 & 0.7 & 1 & 1 & 0 \end{bmatrix}$$

Multiplex network M_B

$$\mathbf{W}_1 = \begin{bmatrix} 0 & 0.35 & 0.35 & 0 & 0 & 0 & 0 \\ 0.35 & 0 & 0.35 & 0.05 & 0 & 0 & 0 \\ 0.35 & 0.35 & 0 & 0 & 0 & 0 & 0 \\ 0 & 0.05 & 0 & 0 & 0.5 & 0.5 & 0 \\ 0 & 0 & 0 & 0.5 & 0 & 0.5 & 0.5 \\ 0 & 0 & 0 & 0.5 & 0.5 & 0 & 0.5 \\ 0 & 0 & 0 & 0 & 0.5 & 0.5 & 0 \end{bmatrix} \quad \mathbf{W}_2 = \begin{bmatrix} 0 & 0.5 & 0.5 & 0.5 & 0.4 & 0 & 0.45 \\ 0.5 & 0 & 0.5 & 0.5 & 0.4 & 0.45 & 0 \\ 0.5 & 0.5 & 0 & 0.5 & 0.4 & 0.45 & 0.5 \\ 0.5 & 0.5 & 0.5 & 0 & 0 & 0 & 0.4 \\ 0.4 & 0.4 & 0.4 & 0 & 0 & 0.4 & 0.4 \\ 0 & 0.45 & 0.45 & 0 & 0.4 & 0 & 0.4 \\ 0.45 & 0 & 0.5 & 0.4 & 0.4 & 0.4 & 0 \end{bmatrix}$$

Multiplex network M_C

$$\mathbf{W}_1 = \begin{bmatrix} 0 & 0.35 & 0.35 & 0 & 0 & 0 & 0 \\ 0.35 & 0 & 0.35 & 0.05 & 0 & 0 & 0 \\ 0.35 & 0.35 & 0 & 0 & 0 & 0 & 0 \\ 0 & 0.05 & 0 & 0 & 0.5 & 0.5 & 0 \\ 0 & 0 & 0 & 0.5 & 0 & 0.5 & 0.5 \\ 0 & 0 & 0 & 0.5 & 0.5 & 0 & 0.5 \\ 0 & 0 & 0 & 0 & 0.5 & 0.5 & 0 \end{bmatrix} \quad \mathbf{W}_2 = \begin{bmatrix} 0 & 0.5 & 0.5 & 0.5 & 0.4 & 0 & 0.45 \\ 0.5 & 0 & 0.5 & 1 & 0.4 & 0.45 & 0 \\ 0.5 & 0.5 & 0 & 0.2 & 0.4 & 0.45 & 0.5 \\ 0.5 & 1 & 0.2 & 0 & 0 & 0 & 0.4 \\ 0.4 & 0.4 & 0.4 & 0 & 0 & 0.4 & 0.4 \\ 0 & 0.45 & 0.45 & 0 & 0.4 & 0 & 0.4 \\ 0.45 & 0 & 0.5 & 0.4 & 0.4 & 0.4 & 0 \end{bmatrix}$$

Appendix C. Toy examples

In this section, we illustrate the proposed method to discover the mesoscale structure of three simple networks with different topologies. Indeed, the topological structure of the layers influences not only the value of ω^*, but also the community partition detected by the procedure.

We consider three alternative weighted multiplex networks (M_A, M_B and M_C) with seven nodes and two layers. Their adjacency matrices are reported in Table 5.

In all three multiplexes, the network in the first layer is the same, and the multiplexes differ only in connections and weights of the second layer. The weighted supradjacency matrix of each multiplex is structured as:

$$\mathcal{W} = \begin{bmatrix} \mathbf{W}_1 & \mathbf{C}_{12} \\ \mathbf{C}_{21} & \mathbf{W}_2 \end{bmatrix},$$

where $\mathbf{W}_1$ and $\mathbf{W}_2$ are the adjacency matrices of the two layers and $\mathbf{C}_{12} = \mathbf{C}_{21} = \omega\mathbf{I}$.

In each network, the first layer is characterized by a strong mesoscale structure identified by two communities: $Cl_{1,1} = \{1, 2, 3\}$ and $Cl_{1,2} = \{4, 5, 6, 7\}$. Both communities have high internal link weights, equal to 0.35 and 0.5 for each existing link between nodes in $Cl_{1,1}$ and $Cl_{1,2}$, respectively. The two clusters are connected to each other only by the link between nodes 2 and 4 with a low weight (equal to 0.05).

We conduct a comparative analysis between the three networks varying connections and weights in the second layer to better enhance the possible effects of ω^*. To this end, we perform on each network a community detection based on the methodology described in Sect. 3.2 considering two alternative cases: $\omega = 0$ and $\omega = \omega^*$[10]. As stressed in the previous section, those values of ω refer to two distinct cases, namely disconnected (or independent) and optimally distant layers, respectively. First of all, we stress that when a layer is characterized by a strong mesoscale structure, the same community partition is obtained in both cases. This is the case of the network in layer 1 of our examples.

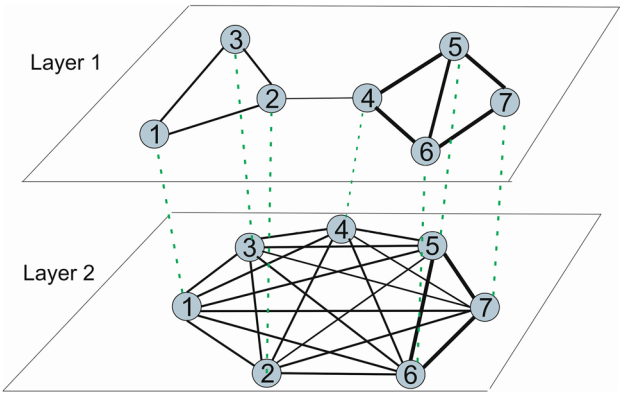

Fig. 7 Weighted undirected multiplex network M_A. The thickness of edges is proportional to the weights

Disruptive effect

We start considering the multiplex M_A displayed in Fig. 7. In the second layer, an easily identifiable mesoscale structure is not present. Indeed, the layer contains a complete subgraph with the same link weights (equal to 0.7) except for nodes 5, 6, and 7 that are connected by links with weights equal to 1. Results of the community detection are reported in Table 6 and graphically shown in Fig. 8. Considering the layers as independent (i.e. $\omega = 0$), two communities emerge in the second layer, namely $Cl_{2,1} = \{1, 2, 3, 4\}$ and $Cl_{2,2} = \{5, 6, 7\}$ (see Fig. 8a). As expected, strongly connected nodes are grouped in a separate cluster $Cl_{2,2}$, while the remaining nodes, connected by links with the same weight, belong to $Cl_{2,1}$.

[10] The optimal value ω^* is obtained by applying the procedure described in Sect. 3.1.

Table 6 Results of the community detection for M_A

	Layer 1		Layer 2	
	Single-layer case	Multiplex case	Single-layer case	Multiplex case
Cluster 1	1, 2, 3	1, 2, 3	1, 2, 3, 4	1
Cluster 2	4, 5, 6, 7	4, 5, 6, 7	5, 6, 7	2
Cluster 3	//	//	//	3
Cluster 4	//	//	//	4
Cluster 5	//	//	//	5, 6, 7

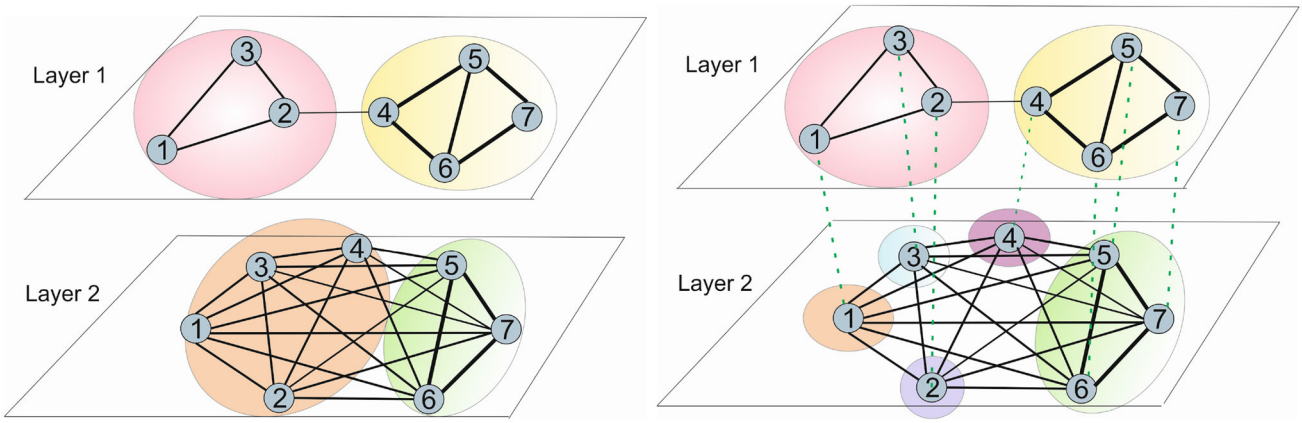

(a) Community detection with $\omega = 0$

(b) Community detection with $\omega = \omega^*$

Fig. 8 Impact of ω on the community detection of the multiplex network M_A

The proposed procedure for the identification of the community structure provides an optimal value of ω equal to 0.95 and reveals useful insights. The community $Cl_{2,1}$ detected by using $\omega = 0$ and characterized by nodes connected with a lower weight, is now decomposed into four singletons, as displayed in Fig. 8b. In turn, the community $Cl_{2,2}$ is preserved. Indeed, the information incorporated in ω^* carefully filters the mesoscale structure highlighting which links are the most significant (or strong) on each layer considering the information flow circulating in the multiplex. In other words, when handling with a multiplex, the connections between layers can modify the relevance of links in the layers because of ω^*. The detected clusters depend indeed on the values assumed by the weights in the layer with respect to ω^*.

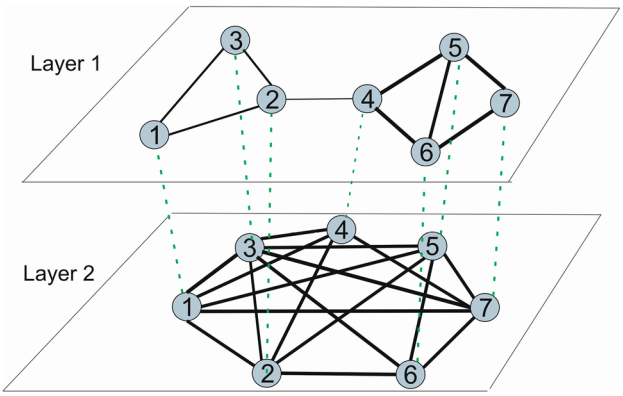

Fig. 9 Weighted undirected multiplex network M_B. The thickness of edges is proportional to the weights

Aggregating effect

In this second example, we consider the multiplex network M_B displayed in Fig. 9. The second layer is slightly modified with respect to the the network M_A. Indeed, edges (1, 6), (2, 7) and (4, 5) have been removed and weights of the remaining links range between 0.4 and 0.5. Notice that also in this case there is not a identifiable community structure, as almost all nodes are connected to each other.

Communities detected are presented in Table 7 and graphically in Fig. 10. According to $\omega = 0$, we obtain a fragmented structure with four communities: $Cl_{2,1} = \{1, 2, 4\}$, $Cl_{2,2} = \{3\}$, $Cl_{2,3} = \{5, 6\}$ and $Cl_{2,4} = \{7\}$ (Fig. 10a). A different grouping is instead obtained when the optimal value of ω^* is considered (Fig. 10b). For the network M_B, we have $\omega^* = 0.5$ and a large cluster including nodes that strongly communicate to each other. In particular, cluster $Cl_{2,1} = \{1, 2, 3, 4, 7\}$ involves the subgraph of the first four

Table 7 Results of the community detection for network M_B

	Layer 1		Layer 2	
	Single-layer case	Multiplex case	Single-layer case	Multiplex case
Cluster 1	1, 2, 3	1, 2, 3	1, 2, 4	1, 2, 3, 4, 7
Cluster 2	4, 5, 6, 7	4, 5, 6, 7	3	5, 6
Cluster 3	//	//	5, 6	//
Cluster 4	//	//	7	//

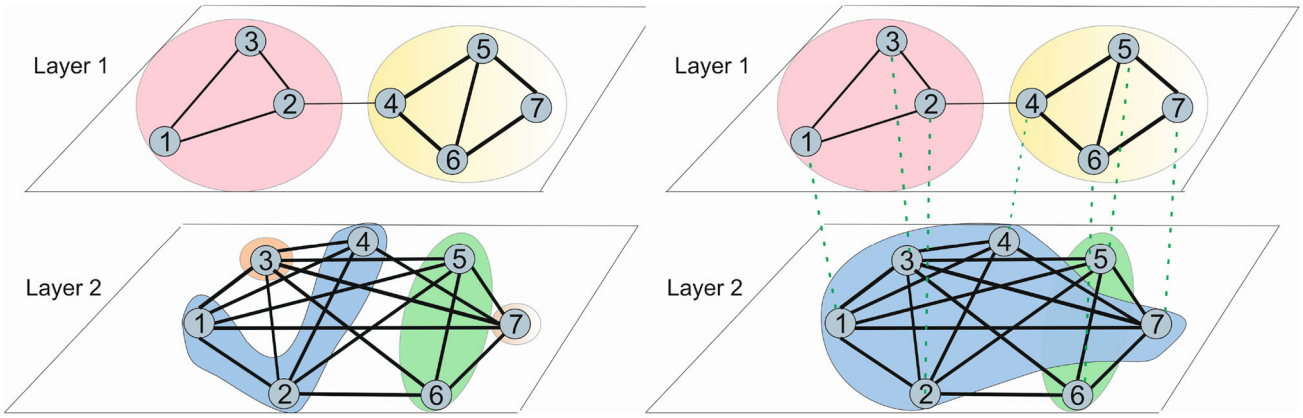

(a) Community detection with $\omega = 0$.

(b) Community detection with $\omega = \omega^*$

Fig. 10 Impact of ω on the community detection of the multiplex network M_B

nodes, that is complete and has all links associated the maximum weighs observed in the network. Node 7 is also included since its connections with the other nodes are, on average, weighted more than the connections with nodes 5 and 6, that are grouped together in a separate cluster. Indeed, these two nodes have not strong enough connections (in terms of weights) with the other ones, but, at the same time, ω^* is not so high to break the connections between them.

Total or partial disruption of communities

This final example has two purposes. First, we show how ω^* changes according to a small variation in the topology of the multiplex. Secondly, we focus on the disruptive effect on the network of this parameter. To this end, we consider the multiplex network M_C (see Fig. 11). With respect to the multiplex M_B, we modified only the weight of two links. Weight $w_{24,2}$ of the link (2, 4) increases by 0.5 while weight $w_{34,2}$ of the link (3, 4) decreases by 0.2. Those little variations change the optimal value of ω, which moves from 0.5 to 0.55. This first result emphasizes the strict connection between the topological structure of the layers and the optimal weight ω^*.

As regards the community structure (see Fig. 12 and Table 8), we observe that, with $\omega = 0$, three main communities emerge on the second layer: $Cl_{2,1} = \{1, 2, 4\}$, $Cl_{2,2} = \{3, 5, 6\}$ and $Cl_{2,3} = \{7\}$. First of all, we notice that, unlike

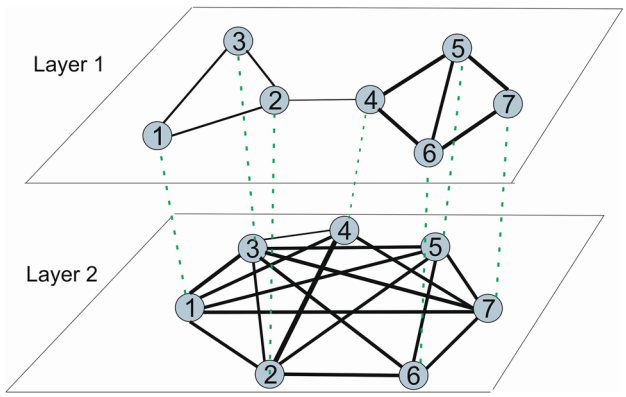

Fig. 11 Weighted undirected multiplex network M_C. The thickness of edges is proportional to the weights

network M_B, node 3 belongs to the same community of nodes 5 and 6. This could be explained by noting that the average weight of the links between nodes 3, 5, 6 is greater than the average weight between nodes 1, 2, 3, 4.

When the optimal value $\omega^* = 0.55$ is considered, the communities, detected with $\omega = 0$, are partially or completely destroyed. It is noticeable that the increase in the optimal value leads to preserve only one connection. We have indeed that all the communities are composed by isolated nodes except for the group made by nodes 2 and 4. The reason

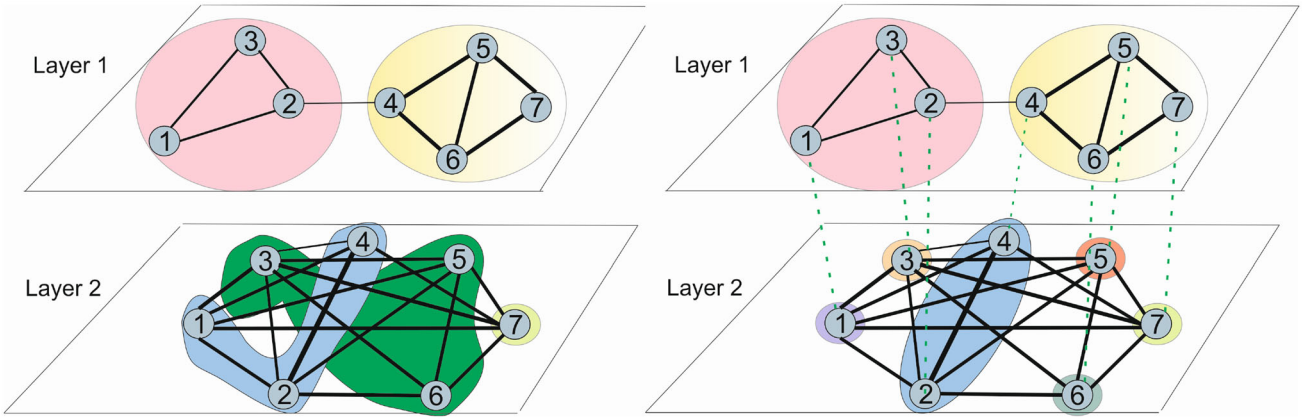

(a) Community detection with $\omega = 0$.

(b) Community detection with $\omega = \omega^*$

Fig. 12 Impact of ω on the community detection of multiplex network M_C

Table 8 Results of the community detection for the multiplex M_C

	Layer 1		Layer 2	
	Single-layer case	Multiplex case	Single-layer case	Multiplex case
Cluster 1	1, 2, 3	1, 2, 3	1, 2, 4	1
Cluster 2	4, 5, 6, 7	4, 5, 6, 7	3, 5, 6	2, 4
Cluster 3	//	//	7	3
Cluster 4	//	//	//	5
Cluster 5	//	//	//	6
Cluster 6	//	//	//	7

why this happens is that the link $(2, 4)$ cannot be broken since ω^* is lower than the weight of that link.

Appendix D. List of countries

Country	Code	Country	Code
Argentina	ARG	Australia	AUS
Azerbaijan	AZE	Belarus	BLR
Belgium	BEL	Bolivia	BOL
Brazil	BRA	Bulgaria	BGR
Canada	CAN	China	CHN
Colombia	COL	Denmark	DNK
Domenican Republic	DOM	Ecuador	ECU
Egypt	EGY	Finland	FIN
Germany	DEU	Greece	GRC
Guatemala	GTM	Hungary	HUN
India	IND	Indonesia	IDN
Ireland	IRL	Israel	ISR
Italy	ITA	Japan	JPN
Kenya	KEN	Lithuania	LTU
Luxembourg	LUX	Malaysia	MYS
Mexico	MEX	Morocco	MAR
Netherlands	NLD	Norway	NOR
Peru	PER	Philippines	PHL
Poland	POL	Portugal	PRT
Qatar	QAT	Romania	ROU
Senegal	SEN	Republic of Serbia	SRB
Singapore	SGP	Slovakia	SVK
South Africa	ZAF	Spain	ESP
Sweden	SWE	Switzerland	CHE
Ukraine	UKR	United Kingdom	GBR
United States of America	USA		

Appendix E. Layers representation

This section collects the layers representation. Opacity of the links is proportional to the absolute value of the correlation coefficient. We report in blue distances related to positive correlations and in red distances related to negative correlations.

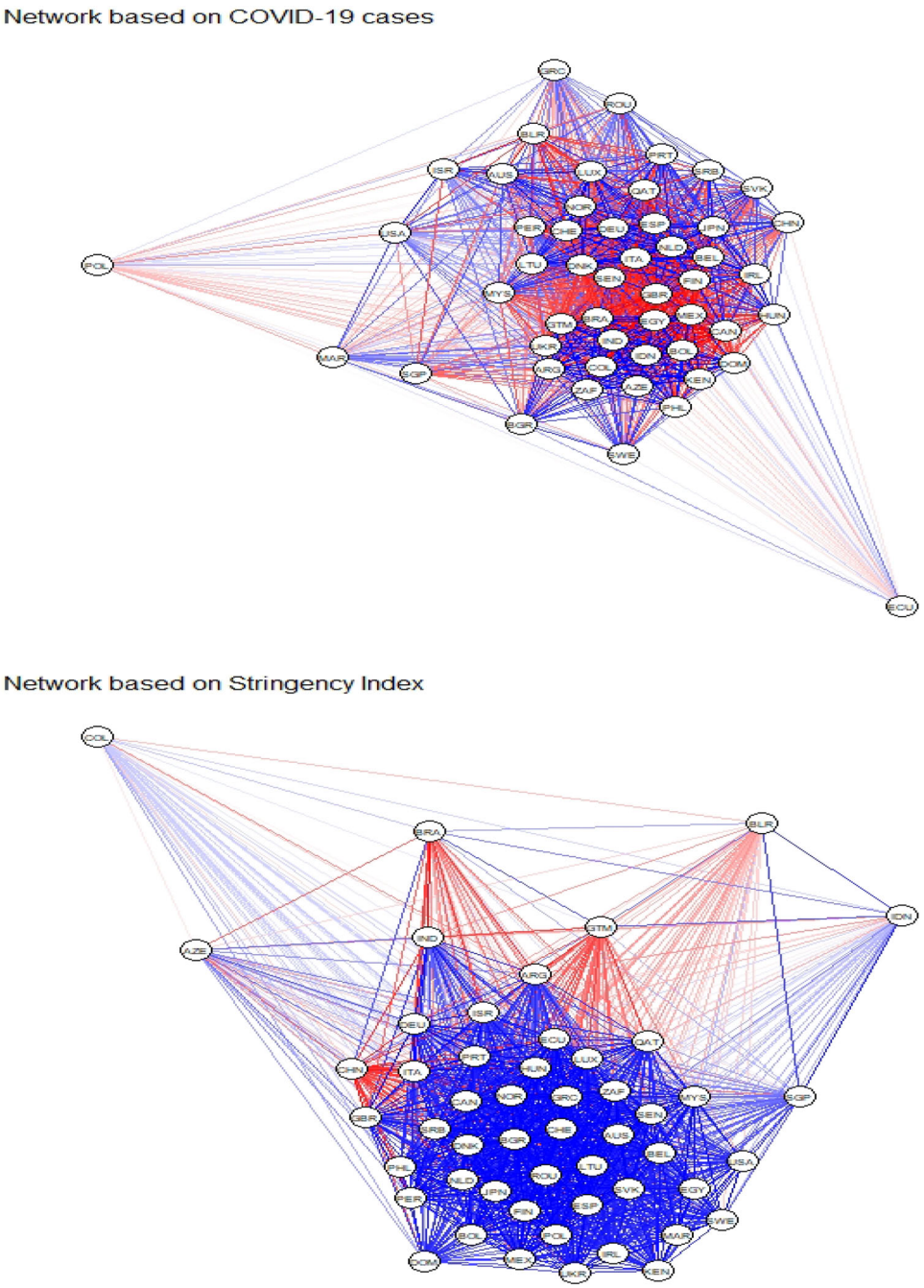

Fig. 13 Figures display COVID-19 and Stringency Index single-layer networks built assuming a weighted adjacency matrix equal to $\mathbf{W}_\alpha$, with $\alpha = 1, 2$

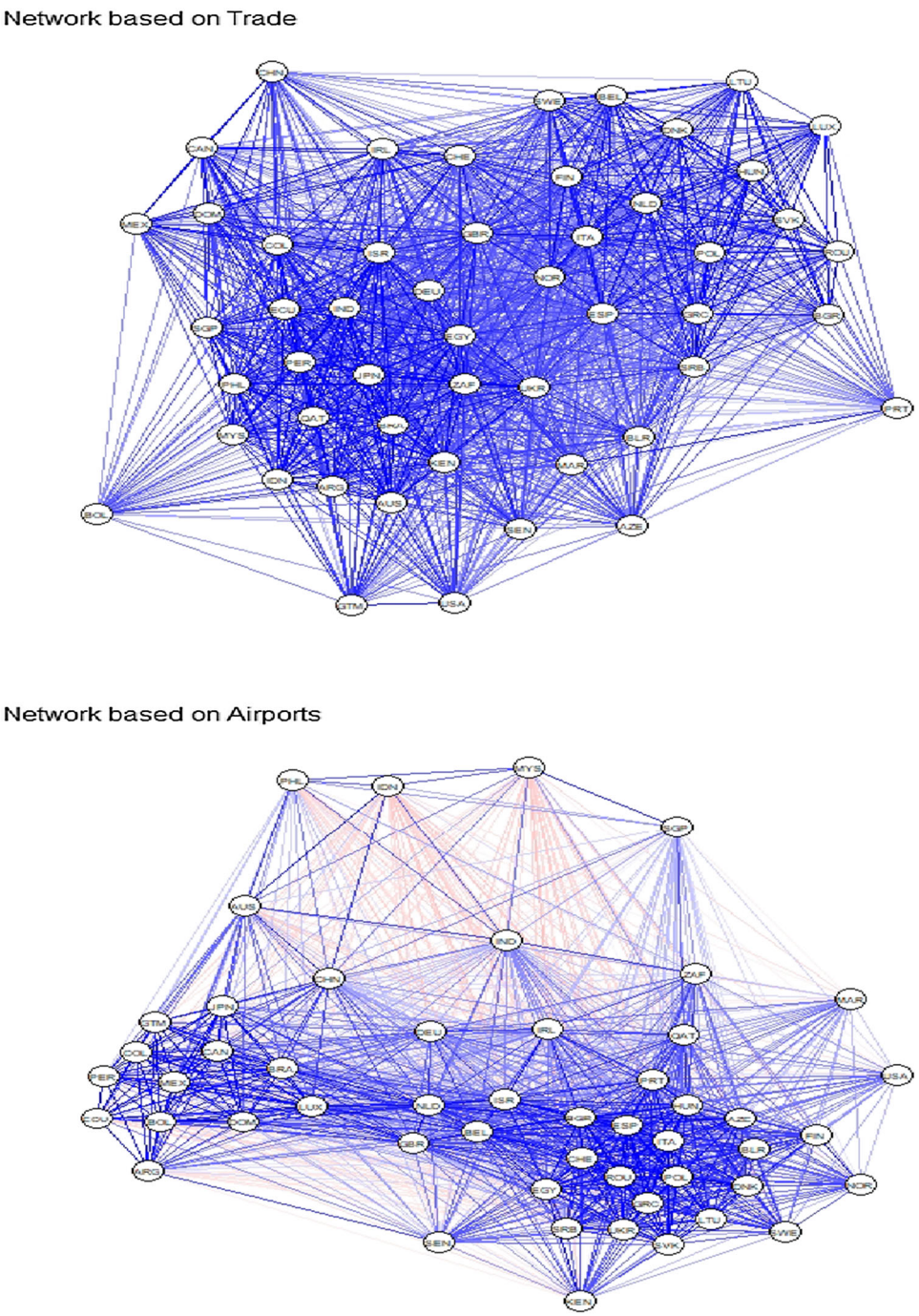

Fig. 14 Figures display the International trade and International air mobility single-layer networks built assuming a weighted adjacency matrix equal to $\mathbf{W}_\alpha$, with $\alpha = 3, 4$

References

Al-Salem W, Moraga P, Ghazi H, Madad S, Hotez PJ (2021) The emergence and transmission of COVID-19 in European countries 2019–2020: a comprehensive review of timelines, cases and containment. Int Health 13(5):383–398. https://doi.org/10.1093/inthealth/ihab037

Amelio A, Pizzuti C (2015) Is normalized mutual information a fair measure for comparing community detection methods? In: ASONAM '15: Proceedings of the 2015 IEEE/ACM International Conference on Advances in Social Networks Analysis and Mining 2015

Antonietti R, De Masi G, Ricchiuti G (2020) Linking FDI network topology with the COVID-19 pandemic. Technical report. Papers in Evolutionary Economic Geography n. 20.54

Antonietti R, Falbo P, Fontini F (2021) The wealth of nations and the first wave of COVID-19 diffusion. Ital Econ J. https://doi.org/10.1007/s40797-021-00174-z

Antonietti R, Falbo P, Fontini F, Grassi R, Rizzini G (2022) The world trade network: country centrality and the COVID-19 pandemic. Appl Netw Sci. https://doi.org/10.1007/s41109-022-00452-4

Baig AS, Butt HA, Haroon O, Rizvi SAR (2021) Deaths, panic, lockdowns and US equity markets: the case of COVID-19 pan-

demic. Financ Res Lett 38:101701. https://doi.org/10.1016/j.frl.2020.101701
Baldwin R, Evenett S (2020) COVID-19 and trade policy: why turning inward won't work. Cepr Press
Barbero J, de Lucio JJ, Rodríguez-Crespo E (2021) Effects of COVID-19 on trade flows: measuring their impact through government policy responses. PLoS ONE 16(10):e0258356. https://doi.org/10.1371/journal.pone.0258356
Barrat A, Barthélemy M, Pastor-Satorras R, Vespignani A (2004) The architecture of complex weighted networks. Proc Natl Acad Sci 101(11):3747–3752
Bartesaghi P, Clemente GP, Grassi R (2022) Community structure in the World Trade Network based on communicability distances. J Econ Interact Coord. https://doi.org/10.1007/s11403-020-00309-y
Boginski V, Butenko S, Pardalos PM (2005) Statistical analysis of financial networks. Comput Stat Data Anal 48(2):431–443
Bown CP (2020) COVID-19: demand spikes, export restrictions, and quality concerns imperil poor country access to medical supplies. In: Baldwin R, Evenett S (eds) COVID-19 and trade policy: why turning inward won't work. CEPR press, Berlin, pp 31–48
Chang C, Liao W, Chen Y, Liou L (2016) A mathematical theory for clustering in metric spaces. IEEE Trans Netw Sci Eng 3(1):2–16. https://doi.org/10.1109/TNSE.2016.2516339
Claeson M, Hanson S (2021) COVID-19 and the Swedish enigma. Lancet 397(10271):259–261. https://doi.org/10.1016/S0140-6736(20)32750-1
Cozzo E, De Arruda GF, Rodrigues FA, Moreno Y (2018) Multiplex networks: basic formalism and structural properties. Springer
Crofts JJ, Higham DJ (2009) A weighted communicability measure applied to complex brain networks. J R Soc Interface 6(33):411–414. https://doi.org/10.1098/rsif.2008.0484
Cross M, Ng SK, Scuffham P (2020) Trading health for wealth: the effect of COVID-19 response stringency. Int J Environ Res Public Health. https://doi.org/10.3390/ijerph17238725
Danon L, Díaz-Guilera A, Duch J, Arenas A (2005) Comparing community structure identification. J Stat Mech Theory Exp 2005(09):9008. https://doi.org/10.1088/1742-5468/2005/09/p09008
De Vico Fallani F, Latora V, Chavez M (2017) A topological criterion for filtering information in complex brain networks. PLoS Comput Biol 13(1):e1005305
Estrada E (2012a) Complex networks in the Euclidean space of communicability distances. Phys Rev E 85:066122. https://doi.org/10.1103/PhysRevE.85.066122
Estrada E (2012b) The structure of complex networks: theory and applications. Oxford University Press
Estrada E (2019) Communicability geometry of multiplexes. New J Phys 21(1):015004. https://doi.org/10.1088/1367-2630/aaf8bc
Estrada E, Gómez-Gardeñes J (2014) Communicability reveals a transition to coordinated behavior in multiplex networks. Phys Rev E 89(4):042819. https://doi.org/10.1103/PhysRevE.89.042819
Estrada E, Hatano N (2008) Communicability in complex networks. Phys Rev E 77:036111. https://doi.org/10.1103/PhysRevE.77.036111
Estrada E, Hatano N (2009) Communicability graph and community structures in complex networks. Appl Math Comput 214(2):500–511. https://doi.org/10.1016/j.amc.2009.04.024
Estrada E, Rodriguez-Velazquez JA (2005) Subgraph centrality in complex networks. Phys Rev E 71:056103. https://doi.org/10.1103/PhysRevE.71.056103
Evenett S, Fiorini M, Fritz J, Hoekman B, Lukaszuk P, Rocha N, Ruta M, Santi F, Shingal A (2022) Trade policy responses to the COVID-19 pandemic crisis: evidence from a new data set. World Econ 45(2):342–364. https://doi.org/10.1111/twec.13119
Fagiolo G (2020) Assessing the impact of social network structure on the diffusion of coronavirus disease (COVID-19): a generalized spatial SEIRD model. Technical report. arXiv:2010.11212
Federico S, Ferrari G (2021) Taming the spread of an epidemic by lockdown policies. J Math Econ 93:102453. https://doi.org/10.1016/j.jmateco.2020.102453
Fernández-Villaverde J, Jones CI (2020) Macroeconomic outcomes and COVID-19: a progress report. Brook Pap Econ Act 2020(3):111–166. https://doi.org/10.1353/eca.2020.0034
Giudici P, Sarlin P, Spelta A (2020) The interconnected nature of financial systems: direct and common exposures. J Bank Finance 112:105149. https://doi.org/10.1016/j.jbankfin.2017.05.010
Gordon DV, Grafton RQ, Steinshamn SI (2021) Cross-country effects and policy responses to COVID-19 in 2020: the Nordic countries. Econ Anal Policy 71:198–210. https://doi.org/10.1016/j.eap.2021.04.015
Hale T, Angrist N, Goldszmidt R, Kira B, Petherick A, Phillips T, Webster S, Cameron-Blake E, Hallas L, Majumdar S, Tatlow H (2021) A global panel database of pandemic policies (Oxford COVID-19 Government Response Tracker). Nat Hum Behav 5:529–538. https://doi.org/10.1038/s41562-021-01079-8
Hyde S (2005) Complex networks on hyperbolic surfaces. Phys A 346(1–2):20–26
Kiyota K (2022) The COVID-19 pandemic and the world trade network. J Asian Econ 78:101419
Kok JLC (2020) Short-term trade-off between stringency and economic growth. CEPR Covid Econ 60:172–189
Lancichinetti A, Fortunato S, Kertész J (2008) Detecting the overlapping and hierarchical community structure in complex networks. New J Phys. https://doi.org/10.1088/1367-2630/11/3/033015
Liu X, Ornelas E, Shi H (2022) The trade impact of the COVID-19 pandemic. World Econ 45(12):3751–3779. https://doi.org/10.1111/twec.13279
Ludvigsson J (2020) The first eight months of Sweden's COVID-19 strategy and the key actions and actors that were involved. Acta Paediatr 109:2459–2471. https://doi.org/10.1111/apa.15582
Ma Y, Mishra S, Han K, X, and D. Zhu. (2021) The relationship between time to a high COVID-19 response level and timing of peak daily incidence: an analysis of governments' Stringency Index from 148 countries. Infect Dis Pov. https://doi.org/10.1186/s40249-021-00880-x
Mantegna RN (1999) Hierarchical structure in financial markets. Eur Phys J B-Condens Matter Complex Syst 11:193–197
Mantegna RN, Stanley HE (1999) Introduction to econophysics: correlations and complexity in finance. Cambridge University Press
Marti G, Nielsen F, Bińkowski M, Donnat P (2021) A review of two decades of correlations, hierarchies, networks and clustering in financial markets. In: Nielsen, F. (eds) Progress in Information Geometry. Signals and Communication Technology. Springer, Cham. pp 245–274
Montes-Orozco E, Mora-Gutiérrez RA, De-Los-Cobos-Silva SG, Rincón-García EA, Torres-Cockrell GS, Juárez-Gómez J, Obregón-Quintana B, Lara-Velázquez P, Gutierrez-Andrade M.á (2020) Identification of COVID-19 spreaders using multiplex networks approach. IEEE Access 8:122874–122883. https://doi.org/10.1109/ACCESS.2020.3007726
Nations (2021) United Nations Statistics Division, UN COMTRADE. International Merchandise Trade Statistics. Available online at https://comtrade.un.org. Accessed 25 Jul 2021
Newman ME, Girvan M (2004) Finding and evaluating community structure in networks. Phys Rev E 69(2):026113. https://doi.org/10.1103/PhysRevE.69.026113
Onnela JP, Kaski K, Kertész J (2004) Clustering and information in correlation based financial networks. Eur Phys J B 38:353–362
Paez A, Lopez FA, Menezes T, Cavalcanti R, Pitta M.G.d.R (2020) A spatio-temporal analysis of the environmental correlates of

COVID-19 incidence in Spain. Geogr Anal. https://doi.org/10.1111/gean.12241
Paterlini M (2020) "Closing borders is ridiculous": the epidemiologist behind Sweden's controversial coronavirus strategy. Nature 580:574. https://doi.org/10.1038/d41586-020-01098-x
Reissl S, Caiani A, Lamperti F, Guerini M, Vanni F, Fagiolo G, Ferraresi T, Ghezzi L, Napoletano M, Roventini A (2022) Assessing the economic impact of lockdowns in Italy: a computational input-output approach. Ind Corp Change 31(2):358–409. https://doi.org/10.1093/icc/dtac003
Remuzzi A, Remuzzi G (2021) COVID-19 and Italy: what next? Health Policy 395:1225–1228. https://doi.org/10.1016/S0140-6736(20)30627-9
Rudin W et al (1964) Principles of mathematical analysis, vol 3. McGraw-hill, New York
Schäfer M, Strohmeier M, Lenders V, Martinovic I, Wilhelm M (2014) Bringing up OpenSky A large-scale ADS-B sensor network for research. In: IPSN-14 Proceedings of the 13th International Symposium on information processing in sensor networks, pp 83–94
Sha D, Malarvizhi AS, Liu Q, Tian Y, Zhou Y, Ruan S, Dong R, Carte K, Lan H, Wang Z et al (2020) A state-level socioeconomic data collection of the United States for COVID-19 research. Data 5(4):118. https://doi.org/10.3390/data5040118
Sharma N, Yadav S, Mangla M et al (2021) Geospatial multivariate analysis of COVID-19: a global perspective. GeoJournal. https://doi.org/10.1007/s10708-021-10520-4
Tumminello M, Aste T, Di Matteo T, Mantegna RN (2005) A tool for filtering information in complex systems. Proc Natl Acad Sci 102(30):10421–10426
Villani L, Pastorino R, Ricciardi W, Ioannidis J, Boccia S (2021) Inverse correlates of COVID-19 mortality across European countries during the first versus subsequent waves. BMJ Glob Health 6(8):1–8. https://doi.org/10.1136/bmjgh-2021-006422
Zanin M, Sousa P, Papo D, Bajo R, García-Prieto J, Pozo F.d, Menasalvas E, Boccaletti S (2012) Optimizing functional network representation of multivariate time series. Sci Rep 2(1):1–6